ACS OMEGA

http://pubs.acs.org/journal/acsodf

Article

I_2-Catalyzed Carbonylation of α-Methylene Ketones to Synthesize 1,2-Diaryl Diketones and Antiviral Quinoxalines in One Pot

Lingkai Kong, Jieru Meng, Wenyue Tian, Jiazheng Liu, Xueping Hu, Zhi-Hong Jiang, Wei Zhang, Yanzhong Li,* and Li-Ping Bai*

Cite This: *ACS Omega* 2022, 7, 1380−1394

Read Online

ACCESS | Metrics & More | Article Recommendations | Supporting Information

ABSTRACT: An efficient approach for the synthesis of 1,2-diaryl diketones was developed from readily available α-methylene ketones by catalysis of I_2. In the same oxidation system, a novel one-pot procedure was established for the construction of antiviral and anticancer quinoxalines. The reactions proceeded well with a wide variety of substrates and good functional group tolerance, affording desired compounds in moderate to excellent yields. Quinoxalines 4ca and 4ad inhibited viral entry of SARS-CoV-2 spike pseudoviruses into HEK-293T-ACE2^h host cells as dual blockers of both human ACE2 receptor and viral spike RBD with IC_{50} values of 19.70 and 21.28 μM, respectively. In addition, cytotoxic evaluation revealed that 4aa, 4ba, 4ia, and 4ab suppressed four cancer cells with IC_{50} values ranging from 6.25 to 28.55 μM.

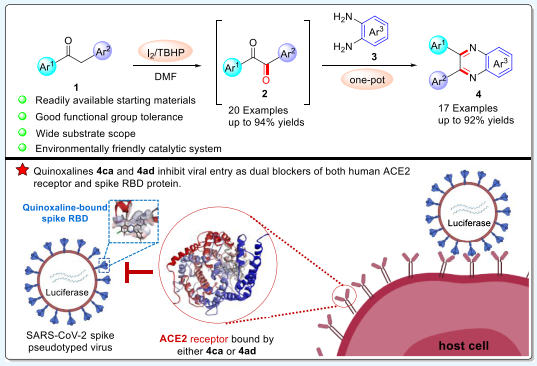

1. INTRODUCTION

1,2-Diaryl diketones are a vital class of organic compounds frequently found in structural units of natural products and bioactive molecules.[1−9] They are also versatile intermediates used in the synthesis of biologically active heterocyclics, such as imidazoles,[10−13] quinoxalines,[14−16] indoles,[17] pyrazines,[18] and triazines.[19−21] Furthermore, 1,2-diaryl diketones could be transformed into greatly important functional materials with electronic and photochemical properties.[22−27] Therefore, various traditional and modern methods for the formation of 1,2-diaryl diketones have been reported, involving the oxidation of α-halo and α-hydroxyl ketones,[28−32] alkene and alkyne oxidation,[33−43] oxidative cleavage of 1,3-diketones,[44−48] benzyl phenyl ketone oxidation,[49−54] oxidative decarboxylative coupling of arylpropiolic/cinnamic acids with arylboronic acids or aryl halides,[55−57] and oxidative rearrangement of α,β-unsaturated diaryl ketones.[58] Among the above methods, the direct oxidation of benzyl phenyl ketone has emerged as a powerfully straightforward strategy to synthesize 1,2-diaryl diketones. In 2012, Alimohammadi et al.[59] reported a chromium reagent 2,6-dicarboxypyridinium fluorochromate-promoted (2,6-DCPFC) method for the oxidation of benzylic C−H bonds into the corresponding carbonyl compounds, but the 2,6-DCPFC was prepared by treatment of aqueous solution of CrO_3 and HF with pyridine 2,6-dicarboxylic acid. Then, Goggiamani et al.[60] disclosed a novel copper-catalyzed oxidation of deoxybenzoins to benzils using PPh_3 as the ligand. Subsequently, a similar copper-catalyzed direct oxidation of C−H bond to synthesize benzils was developed by Wang et al.,[61] in which K_2CO_3 was required as the additive to accelerate the reaction. Additionally, Ravikumar et al.[62] utilized base/DMSO catalytic system for the oxidation of methylene compounds to afford 1,2-diaryl diketones, releasing the environmentally unfriendly and foul-smelling dimethyl sulfide.

Although these methods have generated smoothly the desired compounds, there are still several drawbacks, including the use of noble transition-metal catalysts, complex ligands, high catalyst loading (≥15 mol %), lengthy reaction times, and the tedious preparation of the starting materials. Therefore, from the view of atomic economy and green chemistry, it is still extremely desirable to develop new synthetic approaches for the preparation of 1,2-diaryl diketones under catalytic and metal-free conditions.

To our delight, we developed an efficient and practical method for the oxidative carbonylation of α-methylene ketones into the desired 1,2-diaryl diketones using friendly catalytic system I_2-TBHP (*tert*-butyl hydroperoxide) in DMF (*N*,*N*-dimethylformamide). Gratifyingly, this catalytic transformation was further applied to construct antiviral and anticancer quinoxalines from α-methylene ketones and *o*-phenylenediamines in one pot without any modified reaction conditions,

Received: October 27, 2021
Accepted: December 10, 2021
Published: December 21, 2021

showing good to excellent yields, wide substrate scope, and high functional group tolerance.

2. RESULTS AND DISCUSSION

2.1. Chemistry. Initially, benzyl phenyl ketone **1a** was chosen as the model substrate to explore the oxidation reaction, and the results are shown in Table 1. When the

Table 1. Optimization of the Conditions for the Oxidative Carbonylation of 1a[a]

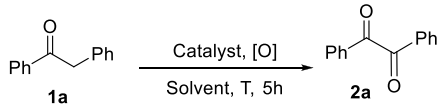

entry	catalyst (mol %)	[O] (equiv)	solvent	T (°C)	yield[b] (%)
1	TBAI (10)	TBHP (3)	DMF	100	29
2	NIS (10)	TBHP (3)	DMF	100	63
3	**I_2 (10)**	**TBHP (3)**	**DMF**	**100**	**87**
4	I_2(50)	TBHP (3)	DMF	100	88
5	I_2(5)	TBHP (3)	DMF	100	82
6	I_2(10)	TBHP (2)	DMF	100	70
7	I_2(10)	TBHP (4)	DMF	100	77
8	I_2(10)	TBHP (3)	DMAc	100	trace
9	I_2(10)	TBHP (4)	NMP	100	trace
10	I_2(10)	TBHP (3)	DMSO	100	51
11	I_2(10)	TBHP (3)	toluene	100	NR
12	I_2(10)	TBHP (3)	1,4-dioxane	100	NR
13	I_2(10)	TBHP (3)	H_2O	100	trace
14	I_2(10)	TBHP (3)	DMF	80	61
15	I_2(10)		DMF	100	trace
16		TBHP (3)	DMF	100	NR

[a]Unless otherwise specified, reactions were carried out using **1a** (0.3 mmol), catalyst (10 mol %), and oxidant (0.9 mmol) in solvent (2.0 mL) at 100 °C. [b]Isolated yields.

reaction of **1a** was carried out in the presence of 10 mol % TBAI using 3.0 equiv of TBHP as the oxidant in DMF at 100 °C for 5 h, the intended benzil **2a** was obtained in only 29% yield (Table 1, entry 1). Subsequently, both NIS and I_2 were examined as catalysts, and it was discovered that utilizing 10 mol % I_2 as a catalyst produced the desired product **2a** in outstanding yield (87%) (Table 1, entries 2−3). The increase of the loading of I_2 afforded a slightly higher yield (88%); however, the decrease of the loading of I_2 gave the product **2a** in a lower yield (Table 1, entries 4−5). From the point of view of economy, 10 mol % I_2 was selected as the catalyst to further optimize the reaction conditions. When the amount of TBHP was 2.0 or 4.0 equiv, the yields of **2a** were decreased to 70 and 77%, respectively (Table 1, entries 6−7). Then, other solvents were also investigated, including DMAc (*N*,*N*-dimethylacetamide), NMP (*N*-methyl-2-pyrrolidone), DMSO (dimethyl sulfoxide), toluene, 1,4-dioxane, and H_2O. It was found that DMF was the most effective one among all tested solvents for this reaction (Table 1, entry 3 vs entries 8−13). Moreover, the yield of **2a** dramatically decreased to 61% at a relatively low temperature of 80 °C (Table 1, entry 14). Notably, no desired product **2a** was obtained in the absence of either TBHP or I_2 (Table 1, entries 15 and 16). Thus, the reaction conditions were optimized as 10 mol % I_2 and 3.0 equiv TBHP in DMF at 100 °C for 5 h (Table 1, entry 3). In comparison to the previously reported literatures,[53,54] our current work had two improvements. One difference is that the amount of catalyst I_2 was reduced from 50 mol % to 10 mol % in the preceding literature. The other advantage is that using DMF as the solvent instead of DMSO avoids the release of the environmentally unfriendly and foul-smelling dimethyl sulfide.

With the optimized reaction conditions in hand (Table 1, entry 3), the scope of the α-methylene ketones was explored (Scheme 1). As a result, various substrates with R^1 bearing electron-donating groups or electron-withdrawing groups were found to generate smoothly the expected products. When the substrates substituted with electron-donating groups R^1 (such as $-CH_3$, $-OCH_3$, $-^tBu$, -3,5-diCH_3) were initially carried out under the standard conditions, the desired products **2b−2g** were obtained in 71%−92% yields. It was worth noting that the substrates containing $-CH_3$ group (R^1) at the meta- and ortho-positions afforded rather good yields of the corresponding products **2e** (86%) and **2f** (81%). Furthermore, the substrate **1h** with phenyl group could be transformed into product **2h** in 80% yield. When the electron-withdrawing groups (R^1 = -Cl, -Br, -F, $-COCH_3$) at the para-positions of aryl rings (Ar^1) were examined, the desired products **2i−2l** were generated in moderate to good yields (48−75%). **2k** (R^1 = F, R^2 = H) and **2l** were, respectively, obtained in only 54 and 48% yields, probably due to the strong electron-withdrawing effect of the -F and $-COCH_3$. Additionally, the effects of -Cl group at meta and ortho substitutions of aryl rings (Ar^1) revealed that the yields gradually fell with the trend of meta and ortho substitutions (**2m**, **2n** vs **2i**). Delightfully, substrates containing naphthalene (**1o**, **1p**), furan (**1q**), and thiophene (**1r**) were also oxidized to the corresponding products **2o**, **2p**, **2q**, and **2r** in 61, 71, 49, and 90% yields, respectively.

Subsequently, we also examined substrates with various functional groups R^2 ($-CH_3$, $-OCH_3$, -Cl, -Br, -F, $-COOCH_3$, $-NO_2$) in this reaction. The results showed that electron-donating groups were more reactive than electron-withdrawing groups substituted on the aryl rings Ar^2 (**2b−2c**, **2e−2f**, **2i−2k**, **2m−2n**, **2s−2t**). When the substrates with electron-donating groups $-CH_3$ and $-OCH_3$ (R^2) were subjected to the reaction conditions, the intended products **2b** and **2c** were acquired in outstanding yields of 94 and 91%, respectively. Further substrate investigations demonstrated that the $-CH_3$ group at the *m*- and *o*-substituents of the Ar^2 produced the respective products **2e** and **2f** in slightly lower yields of 74 and 76%, probably due to the high steric hindrance. While electron-withdrawing functional groups (-Cl, -Br, -F, $-COOCH_3$) on the aryl rings Ar^2 were studied under the standard conditions, the corresponding products (**2i−2k**, **2s**) were prepared in good yields (62−79%). It should be noted that nitro ($-NO_2$) was well tolerated, affording the expected product **2t** in only 37% yield due to the strong electron-withdrawing effect of the $-NO_2$. In addition, substrates with -Cl group (R^2) at the *m*- and *o*-positions of aryl rings Ar^2 were also smoothly converted into the desired products **2m** and **2n** in 61 and 58% yields, respectively. Unfortunately, no desired products were observed when the substrates of acetophenone, acetone, and 2-butanone were used to carry out the reactions under the optimized conditions.

To expand the synthetic potential of our present catalytic protocol, a gram-scale reaction of **1a** was carried out under the optimized conditions, delivering the desired product **2a** in 62% yield (Scheme 2).

Moreover, several control experiments were conducted to explore the mechanism of the reaction (Scheme 3). When the

https://doi.org/10.1021/acsomega.1c06017
ACS Omega 2022, 7, 1380−1394

Scheme 1. Substrate Scope of the α-Methylene Ketones

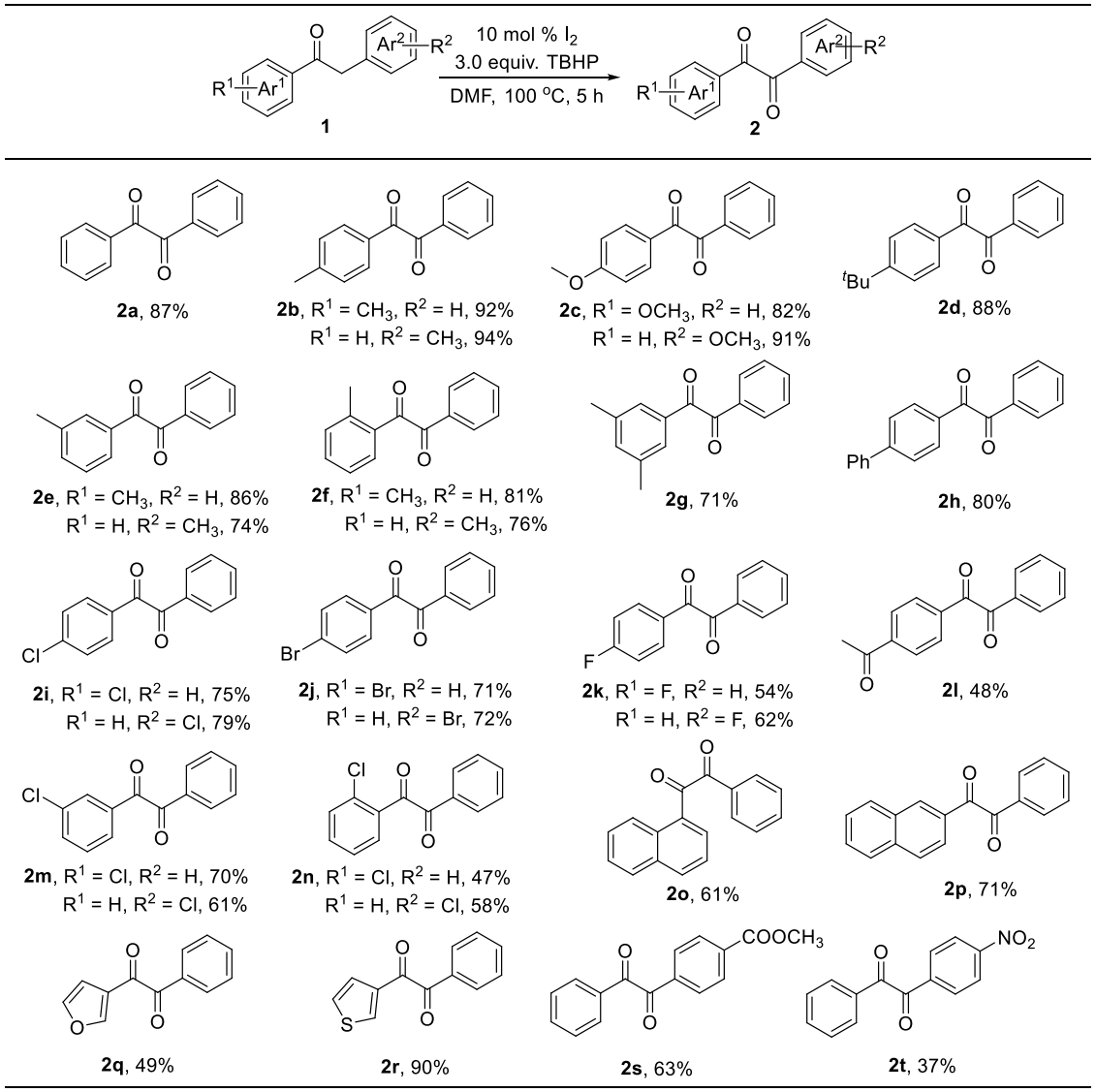

Scheme 2. Gram-Scale Synthesis of Benzil 2a

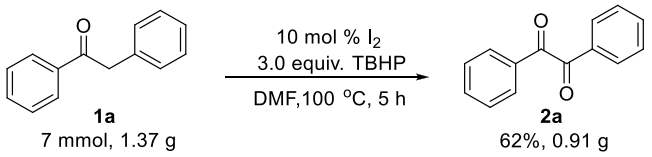

substrates **5** and **6** were employed under the standard reaction conditions, no desired products were observed (Scheme 3a,b), indicating that the presence of the aryl rings in **1** is crucial for the success of this reaction. Under optimized conditions, the reaction was additionally performed in the presence of 1.5 equiv 2,2,6,6-tetramethylpiperidine-1-oxyl (TEMPO) (Scheme 3c) as a radical scavenger without producing any other side products, indicating that no reaction occurred. This result demonstrated that the reaction might include a radical process. The involvement of a radical process was different from that reported in the literature.[37]

Based on the above control experiments and previous literature reports, a possible mechanism was proposed in Scheme 4. Initially, the *tert*-butoxyl and *tert*-butylperoxy radicals (^{t}BuO$^\bullet$ and ^{t}BuOO$^\bullet$) were formed via the redox cycle reaction of I_2 and TBHP.[70−72] Subsequently, the generated *tert*-butoxyl radical (^{t}BuO$^\bullet$) abstracted hydrogen atom from benzyl phenyl ketone **1a** to afford the benzylic radical **I**,[73,74] and it was followed by the reaction of *tert*-butylperoxy radical (^{t}BuOO$^\bullet$) with the intermediate **I** to generate the peroxide intermediate **II**.[75,76] Finally, the intermediate **II** underwent rapid oxidation or a Kornblum−DeLaMare rearrangement to give the desired product **2a** with the elimination of *tert*-butyl alcohol.[70,77−79]

Recently, the synthesis of quinoxalines has also received great attention due to their biological activities, including anti-infectious,[80,81] antidepressant,[82] antitumor,[83−86] anti-inflammatory,[87,88] antibacterial,[89,90] and antimalarial effects.[91] Inspired by the success of the oxidation of α-methylene ketones to benzils **2**, we further tested its applications to construct quinoxaline compounds. Fortunately, quinoxalines[92] were synthesized from α-methylene ketones and *o*-phenylenediamines in one pot under the above standard conditions. To obtain quinoxalines with potential antiviral entry activities against SARS-CoV-2, we initially utilized the molecular docking study to predict the binding interaction of 20

https://doi.org/10.1021/acsomega.1c06017
ACS Omega 2022, 7, 1380−1394

Scheme 3. Control Experiments

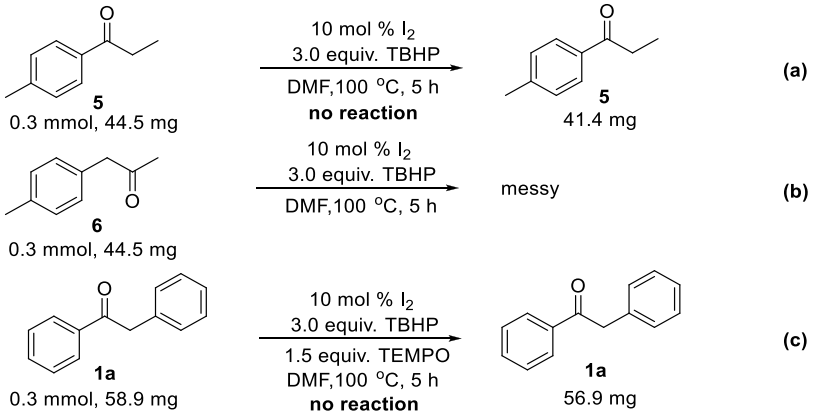

Scheme 4. Proposed Mechanism

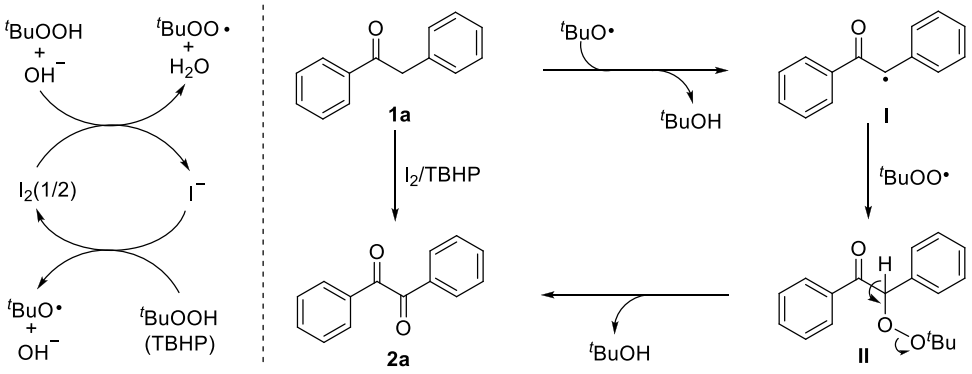

quinoxalines (**4aa**−**4ta** in Scheme S1) with both human ACE2 and SARS-CoV-2 Spike RBD proteins. As a result of the calculated binding energy (Table S1), **4ca** has the lowest binding energy with both ACE2 and Spike RBD proteins while **4ra** possesses the highest energy with both proteins among all 20 quinoxalines. A lower binding energy suggested a more stable interaction between the molecule and the protein. Based on the above molecular docking results, nine representative quinoxalines including **4ca** and **4ra** were selected to be synthesized not only for examining the application of benzils but also for the acquirement of quinoxalines with antiviral entry activities against SARS-CoV-2.

Then, we investigated the scope of the α-methylene ketones and *o*-phenylenediamines, and the results are shown in Scheme 5. Both electron-donating (-CH_3, -OCH_3, -Ph) and electron-withdrawing groups (-Cl, -Br, -F) at the *p*-positions of aryl ring Ar^1 underwent smoothly the oxidation and cyclization reactions in one pot, producing the desired products (**4ba**, **4ca**, **4ha**, **4ia**, **4ja**, **4ka**) in moderate to excellent yields (54−88%). To our delight, the substrates bearing naphthalene and thiophene rings proceeded well to generate the expected products (**4pa**, **4ra**) in good yields (72%−73%). Furthermore, the compatibility and scope of *o*-phenylenediamines **3** were also explored. The reactions of the substrates **3** with electron-donating groups (-CH_3, -OCH_3) and electron-withdrawing groups (-Cl, -CN, -$COOCH_3$) produced the corresponding products **4ab**−**4af** in 78−87% yields. Gratifyingly, the benzyl phenyl ketone **1a** reacted smoothly with 2,3-diaminonaphthalene **3g**, providing **4ag** in 85% yield. Finally, the reactions of benzyl phenyl ketone **1a** and 1,2-bis(4-methoxyphenyl)-ethenone **1u** with 3-methylbenzene-1,2-diamine **3h** were explored under the standard conditions, smoothly giving the desired products **4ah** and **4uh** in 82 and 81% yields, respectively.

2.2. Biological Evaluation. All synthesized quinoxalines **4aa**−**4ca**, **4ha**, **4ia**−**4ka**, **4pa**, **4ra**, and **4ab**−**4ag** were evaluated for their potential to inhibit viral entry of a SARS-CoV-2 spike pseudotyped virus bearing luciferase reporter into HEK-293T-ACE2[h] host cell that highly expresses human ACE2 (angiotensin-converting enzyme 2) receptor (Table 2).[63] Initially, the maximum nontoxic concentration (CC_0) values of all quinoxalines were examined on the host cells of HEK-293T-ACE2[h] by MTT,[93,94] and their antiviral entry activities were subsequently evaluated under the compounds' concentrations no more than the CC_0 values. SARS-CoV-2 antibody was used as a positive inhibitor. 5′,7-Diallyl-3,3′-bis((5-(4-methoxyphenyl)-1,3,4-oxadiazol-2-yl)methyl)-[5,7′-bibenzo[*d*]oxazole]-2,2′(3*H*,3′*H*)-dione (**6p**), a recently reported ACE2 blocker,[63] was employed as a positive antiviral entrance reference. As a result (Table 2 and Figure 1), **4ca**, **4ha**, and **4ad** exhibited antiviral entry effect on SARS-CoV-2 spike pseudoviruses with IC_{50} values of 19.70, 142.50, and 21.28 μM, respectively. Quinoxaline **4ca** exhibited a selectivity index (SI) of 14.05, whereas the SI of **4ad** was higher than 23.49, indicating that **4ad** had a larger safety window between cytotoxicity and antiviral activity than **4ca**. The binding behaviors of **4ca**, **4ha**, and **4ad** with both SARS-CoV-2 spike RBD and human ACE2 protein were also examined by biolayer interferometry (BLI) binding assay (Table 3 and Figure 2). It was found that **4ca**, **4ha**, and **4ad** bind to human ACE2 protein with K_D values of 3.67, 237.90, and 4.02 μM, respectively. With SARS-CoV-2 spike RBD, quinoxalines **4ca**, **4ha**, and **4ad** had

https://doi.org/10.1021/acsomega.1c06017
ACS Omega 2022, 7, 1380−1394

Scheme 5. One-Pot Synthesis of Quinoxalines from α-Methylene Ketones and o-Phenylenediamines

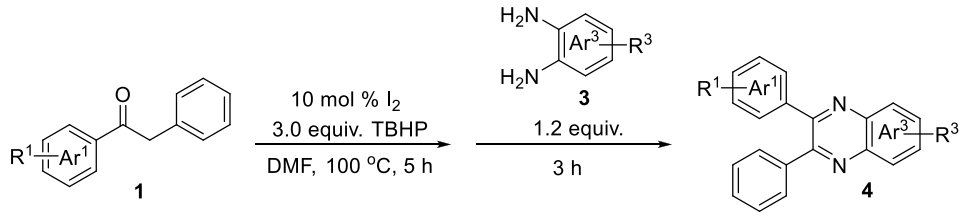

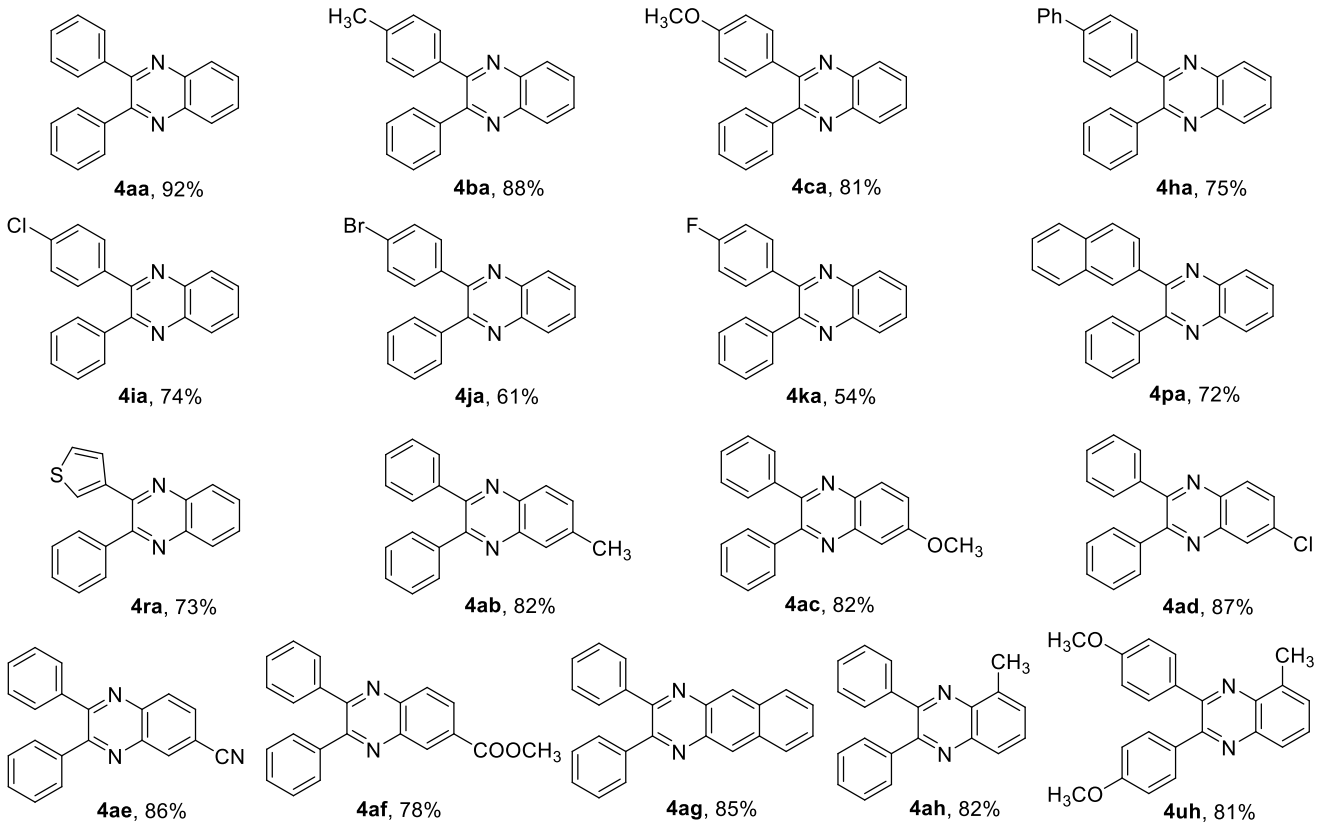

K_D values of 15.48, 135.25, and 8.16 μM, respectively, indicating that both **4ca** and **4ad** had stronger binding affinity with human ACE2 protein than that with spike RBD. Molecular docking study (Table 3 and Figure 3) revealed that **4ca** interacts with the amino acid residues of ASN 394 and TRP 349 in human ACE2 receptor with a calculated CDOCKER interaction energy of −38.4377 kcal/mol, and **4ad** interacts with human ACE2 receptor *via* the sites of TRP 349, TYR 510, and HIS 345 with a CDOCKER interaction energy of −28.8546 kcal/mol. The computed CDOCKER interaction energies of **4ca** and **4ad** with SARS-CoV-2 spike RBD protein were −26.2545 and −22.9192 kcal/mol, respectively. Taken together, quinoxalines **4ca** and **4ad** could prevent SARS-CoV-2 from entering the host cell by dual blocking of both human ACE2 receptor and viral spike RBD.

In addition, all 13 synthesized quinoxalines were further evaluated for their cytotoxicity against four cancer cell lines (MDA-MB-231, MCF-7, T47D, and A549) by the MTT method. As presented in Table 4, it was found that compounds **4aa**, **4ba**, **4ia** and **4ab** exhibited cytotoxic effects on four cancer cell lines of MCF-7, T47D, MDA-MB-231, and A549 with IC_{50} values ranging from 6.25 to 28.55 μM after 72 h treatment. Compound **4ag** displayed IC_{50} values of 20.52, 45.01, and 44.45 μM against T47D, MDA-MB-231, and A549 cancer cells, respectively. Of note, the cytotoxic effect of **4ia** on MCF-7 and T47D cells was 1.96- and 4.27-fold more potent than that of the positive control of berberine,[93] respectively. Quinoxaline **4ab** also displayed 3.94 times stronger cytotoxicity than berberine against T47D cancer cells.

3. CONCLUSIONS

In summary, we have developed a novel I_2-catalyzed oxidative carbonylation of the benzylic Csp^3-H bonds using TBHP as the green oxidant. This method provided rapid and efficient access to 1,2-diaryl diketones from the α-methylene ketones, exhibiting several advantages including easily accessible starting materials, broad substrate scope, and environmentally friendly catalytic system. Moreover, we also established an efficient one-pot process for the construction of biologically active quinoxalines in the same oxidation system. A series of desired compounds were synthesized in good to excellent yields with good functional group tolerance. Quinoxalines **4ca** and **4ad** exhibited potential in suppressing viral entry for SARS-CoV-2 as dual blockers of both human ACE2 receptor and SARS-CoV-2 spike RBD. In addition, quinoxalines **4ia** and **4ab**

https://doi.org/10.1021/acsomega.1c06017
ACS Omega 2022, 7, 1380−1394

Table 2. Antiviral Entry Activities of Quinoxalines for SARS-CoV-2 Spike Pseudovirus into HEK-293T-ACE2h Host Cells

compounds	CC_0[a] (μM)	TC_{50}[b] (μM)	IC_{50}[c] (μM)	SI[d]
4aa	>250	>25	ND[e]	ND[e]
4ba	125	271.67 ± 13.00	ND	ND
4ca	125	276.90 ± 13.45	19.70 ± 1.23	14.05
4ha	>250	>500	142.50 ± 12.45	>3.50
4ia	25	115.20 ± 9.72	ND	ND
4ja	25	>100	ND	ND
4ka	25	>100	ND	ND
4pa	>25	>250	ND	ND
4ra	62.5	337.06 ± 15.49	ND	ND
4ab	62.5	288.40 ± 17.65	ND	ND
4ac	50	116.03 ± 4.28	ND	ND
4ad	>25	>500	21.28 ± 0.44	>23.49
4ae	125	303.27 ± 9.51	ND	ND
4af	100	>100	ND	ND
4ag	50	107.20 ± 1.64	ND	ND
6p[f]	>100	>100	11.90 ± 0.59	>8.40
antibody[g]	0.10	ND	0.032 ± 0.001	ND

[a]CC_0 represents the maximum nontoxic concentration of compounds. [b]TC_{50} means the concentration that caused 50% cells' death. [c]IC_{50} stands for the compounds' concentration that suppressed 50% viral entry into HEK-293T-ACE2[h] host cells. [d]SI represents selectivity index that indicates compounds' window between cytotoxicity and antiviral activity by the ratio of TC_{50}/IC_{50}. [e]ND means not determined. [f]honokiol derivative **6p** (a reported ACE2 blocker). [g]SARS-CoV-2 antibody was utilized as a positive control compound for antiviral entry evaluation.

exhibited cytotoxic effects that were comparable to or better than berberine on three human breast cancer cell lines of MDA-MB-231, MCF-7, and T47D. Further studies are in progress to elucidate the reaction mechanism and applications of the approaches. The inhibitory effect of **4ca** and **4ad** on SARS-CoV-2 viral strains needs further study in a biosafety level 3 facility.

4. EXPERIMENTAL SECTION

4.1. General Details. All reactions were performed in flame-dried glassware in an air condition, unless otherwise noted. Column chromatographic purification of products was carried out using silica gel (200−300 mesh). The commercial reagents were used without further purification. ^{1}H NMR spectra were recorded at 600 MHz, and ^{13}C NMR spectra were measured at 150 MHz in $CDCl_3$ (containing 0.03% TMS) solutions. Tetramethylsilane (δ = 0.00 ppm) and $CDCl_3$ (δ = 77.00 ppm) were used as internal references for ^{1}H NMR and ^{13}C NMR spectra, respectively. High-resolution mass spectra (HRMS) were performed on either an electrospray ionization (ESI) mass spectrometer with a time-of-flight (TOF) analyzer (Agilent 6545 QTOF-MS) or an electrospray ionization (ESI) Fourier transform mass spectrometer (FTMS, Thermo Q-Exactive Focus).

4.2. General Procedure for the Synthesis of Products 2 and 4. Benzyl phenyl ketone **1a** (58.9 mg, 0.3 mmol), I_2 (7.6 mg, 0.03 mmol), and DMF (2 mL) were placed in a Schlenk tube; then, TBHP (70% in water, 124 μL, 0.9 mmol) was added into the above mixture under air. After the completion of the addition, the reaction mixture was allowed to react at 100 °C (oil bath) for 5 h. Subsequently, the reaction mixture was cooled to room temperature, treated with H_2O, saturated sodium thiosulfate solution, and then extracted with ethyl acetate. The combined organic layers were washed with brine and dried over anhydrous Na_2SO_4. After removal of the ethyl acetate under reduced pressure, the residue was purified by column chromatography on silica gel (petroleum ether/ethyl acetate = 20:1) to afford benzil **2a**.

Benzyl phenyl ketone **1a** (58.9 mg, 0.3 mmol), I_2 (7.6 mg, 0.03 mmol), and DMF (2 mL) were added in a Schlenk tube; then, TBHP (70% in water, 124 μL, 0.9 mmol) was supplemented under air. After the completion of the addition, the reaction mixture was allowed to react at 100 °C (oil bath) for 5 h. Subsequently, *o*-phenylenediamine **3a** (38.9 mg, 0.36 mmol) was added at room temperature. Then, the reaction mixture was stirred at 100 °C (oil bath) for 3 h. After the reaction was completed, the reaction mixture was quenched with H_2O and saturated sodium thiosulfate solution and then extracted with ethyl acetate. The combined organic layers were

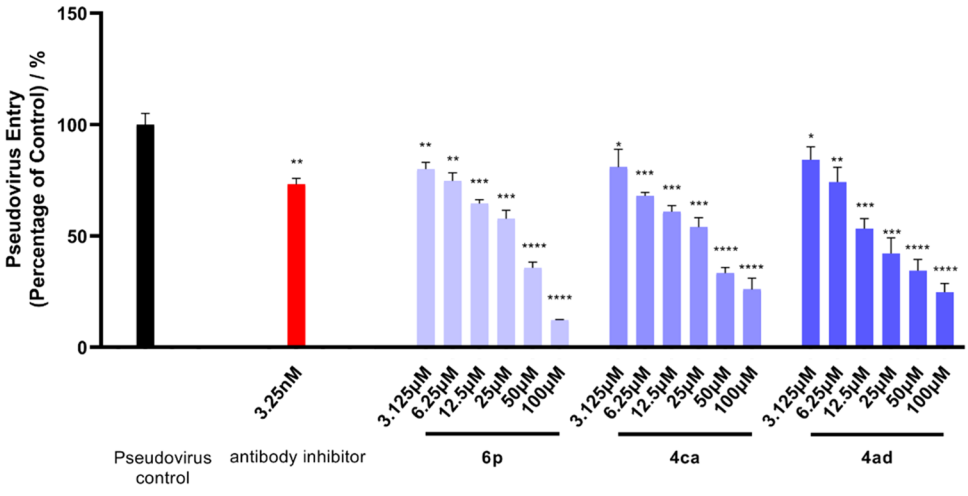

Figure 1. Inhibitory effect of **4ca** and **4ad** on the entry of SARS-CoV-2 pseudovirus to host cells. The luciferase luminescence value was defined as 100% for the pseudovirus control. The values of luminescence of compound-treated groups were normalized accordingly. Data were expressed as mean ± standard error (n = 3). *p < 0.05, **p < 0.01, ***p < 0.001, ****p < 0.0001 compared with pseudovirus control group.

https://doi.org/10.1021/acsomega.1c06017
ACS Omega 2022, 7, 1380−1394

Table 3. Binding Parameters of Selected Quinoxalines with Human ACE2 and SARS-CoV-2 Spike RBD Proteins

	binding with ACE2		binding with spike RBD	
compounds	K_D value[a] (μM)	energy[b] (kcal/mol)	K_D value[a] (μM)	energy[b] (kcal/mol)
4aa	5891.00 ± 1674.28	NC[c]	1000.45 ± 760.90	NC[c]
4ca	3.67 ± 0.66	−38.4377	15.48 ± 1.14	−26.2545
4ha	237.90 ± 57.28	NC	135.25 ± 17.75	NC
4ad	4.02 ± 2.03	−28.8546	8.16 ± 1.34	−22.9192

[a]K_D means equilibrium dissociation constant of compounds with protein by BLI binding assay. [b]Energy is the calculated CDOCKER interaction energy. [c]NC means not computed.

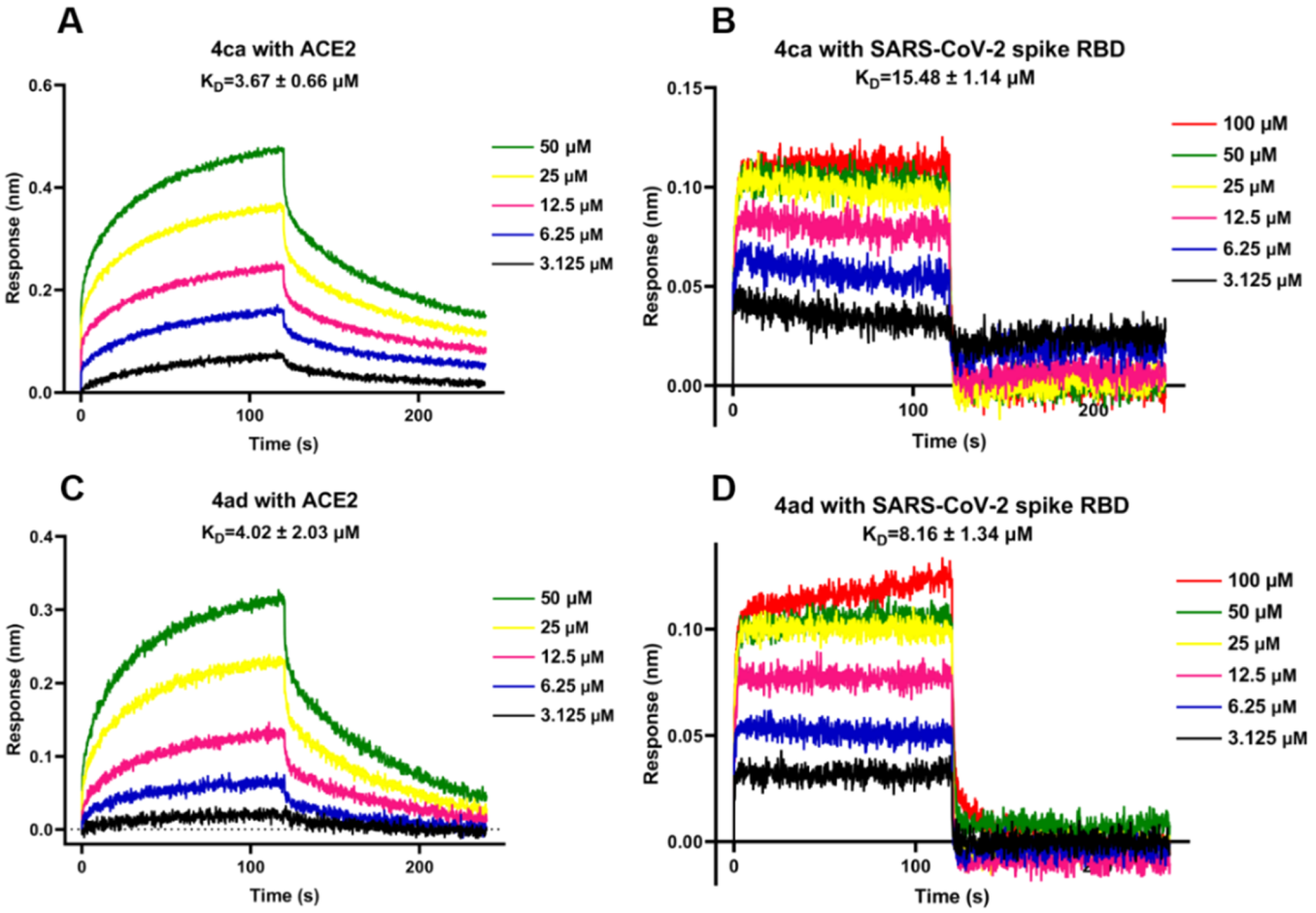

Figure 2. Binding curves of **4ca** and **4ad** with human ACE2 and SARS-CoV-2 spike RBD proteins by BLI binding assay. (A) **4ca** with ACE2. (B) **4ca** with SARS-CoV-2 spike RBD. (C) **4ad** with ACE2. (D) **4ad** with SARS-CoV-2 spike RBD.

washed with brine and dried over anhydrous Na_2SO_4. After removal of the ethyl acetate under reduced pressure, the residue was purified by column chromatography on silica gel (petroleum ether/ethyl acetate = 50:1−20:1) to afford 2,3-diphenylquinoxaline **4aa**.

*4.2.1. Benzil (**2a**).* Yellow solid (54.8 mg, 87% yield), purified by column chromatography on silica gel (petroleum ether/ethyl acetate = 20:1). ^{1}H NMR (600 MHz, $CDCl_3$) δ 7.49−7.52 (m, 4H), 7.63−7.67 (m, 2H), 7.97 (dd, J_1 = 8.4 Hz, J_2 = 1.2 Hz, 4H); ^{13}C NMR (150 MHz, $CDCl_3$) δ 128.99, 129.84, 132.94, 134.86, 194.55. HRMS (ESI) m/z $[M + H]^+$ calcd for $C_{14}H_{11}O_2$ 211.0754, found 211.0761.

*4.2.2. 1-Phenyl-2-(p-tolyl)ethane-1,2-dione (**2b**).* Yellow oil (61.9 mg, 92% yield, from 1, R^1 = CH_3, R^2 = H), (63.5 mg, 94% yield, from 1, R^1 = H, R^2 = CH_3), purified by column chromatography on silica gel (petroleum ether/ethyl acetate = 50:1-20:1). ^{1}H NMR (600 MHz, $CDCl_3$) δ 2.42 (s, 3H), 7.30 (d, J = 8.4 Hz, 2H), 7.48−7.51 (m, 2H), 7.62−7.65 (m, 1H), 7.86 (d, J = 8.4 Hz, 2H), 7.96 (dd, J_1 = 8.1 Hz, J_2 = 1.2 Hz, 2H); ^{13}C NMR (150 MHz, $CDCl_3$) δ 21.85, 128.92, 129.70, 129.81, 129.95, 130.52, 133.03, 134.74, 146.18, 194.28, 194.74. HRMS (ESI) m/z $[M + H]^+$ calcd for $C_{15}H_{13}O_2$ 225.0910, found 225.0918.

*4.2.3. 1-(4-Methoxyphenyl)-2-phenylethane-1,2-dione (**2c**).* Yellow oil (58.9 mg, 82% yield, from **1**, R^1 = OCH_3, R^2 = H), (65.9 mg, 91% yield, from **1**, R^1 = H, R^2 = OCH_3), purified by column chromatography on silica gel (petroleum ether/ethyl acetate = 50:1−20:1). ^{1}H NMR (600 MHz, $CDCl_3$) δ 3.87 (s, 3H), 6.97 (d, J = 8.4 Hz, 2H), 7.47−7.51 (m, 2H), 7.61−7.65 (m, 1H), 7.93−7.98 (m, 4H); ^{13}C NMR (150 MHz, $CDCl_3$) δ 55.56, 114.30, 125.97, 128.88, 129.78,

https://doi.org/10.1021/acsomega.1c06017
ACS Omega 2022, 7, 1380−1394

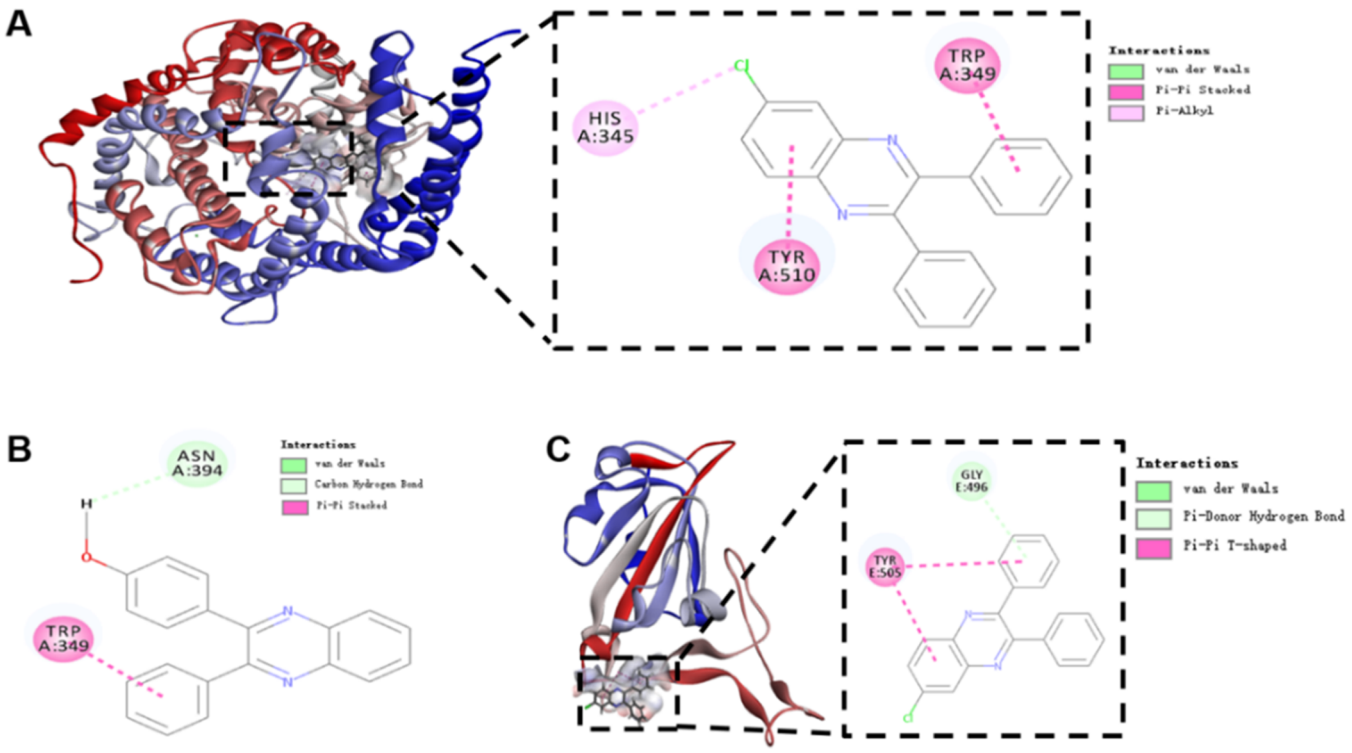

Figure 3. Docking simulation of quinoxalines **4ad** (A, C) and **4ca** (B) in the active sites of human ACE2 (PDB code: 1R4L) and SARS-CoV-2 spike RBD (PDB code: 6M0J). (A) 3D and 2D interaction model of **4ad** (in gray) with human ACE2 receptor. (B) 2D interaction model of **4ca** with human ACE2 receptor. (C) 3D and 2D interaction model of **4ad** (in gray) with SARS-CoV-2 spike RBD protein.

Table 4. Cytotoxic Activities of 13 Quinoxalines against Four Human Cancer Cell Lines for 72 h

	IC_{50} (μM)			
compounds	MCF-7	T47D	MDA-MB-231	A549
4aa	16.68 ± 1.34	11.36±1.17	28.55 ± 1.85	26.31 ± 1.96
4ba	15.65 ± 1.18	9.76 ± 1.30	21.45 ± 1.19	24.06 ±1.11
4ca	>50	>50	48.84 ± 1.01	>50
4ha	>50	>50	>50	>50
4ia	7.30 ± 1.10	6.25 ± 0.73	17.75 ±0.69	18.55 ±0.25
4pa	>50	>50	>50	>50
4ra	>50	>50	>50	>50
4ab	10.01 ± 0.55	6.77 ± 0.57	18.21 ± 1.34	19.72 ± 1.28
4ac	>50	>50	>50	>50
4ad	>50	>50	>50	>50
4ae	>50	>50	>50	>50
4af	>50	>50	>50	>50
4ag	>50	20.52 ± 1.64	45.01 ± 1.57	44.45 ± 3.55
berberine[a]	14.32 ± 1.44	26.69 ± 2.45	17.96 ± 1.91	5.22 ± 0.44

[a]Berberine was used as the positive control.

132.28, 133.10, 134.66, 164.94, 193.12, 194.82. HRMS (ESI) m/z $[M + H]^+$ calcd for $C_{15}H_{13}O_3$ 241.0859, found 241.0866.

*4.2.4. 1-(4-(tert-Butyl)phenyl)-2-phenylethane-1,2-dione (**2d**).* Yellow oil (70.4 mg, 88% yield), purified by column chromatography on silica gel (petroleum ether/ethyl acetate = 50:1−20:1). ^{1}H NMR (600 MHz, $CDCl_3$) δ 1.34 (s, 9H), 7.48−7.51 (m, 2H), 7.53 (d, J = 8.4 Hz, 2H), 7.62−7.65 (m, 1H), 7.91 (d, J = 8.4 Hz, 2H), 7.96−7.98 (m, 2H); ^{13}C NMR (150 MHz, $CDCl_3$) δ 30.90, 35.32, 126.00, 128.92, 129.83, 129.84, 130.42, 133.05, 134.72, 158.97, 194.26, 194.75. HRMS (ESI) m/z $[M + H]^+$ calcd for $C_{18}H_{19}O_2$ 267.1380, found 267.1390.

*4.2.5. 1-Phenyl-2-(m-tolyl)ethane-1,2-dione (**2e**).* Yellow solid (58.1 mg, 86% yield, from **1**, R^1 = CH_3, R^2 = H), (49.8 mg, 74% yield, from **1**, R^1 = H, R^2 = CH_3), purified by column chromatography on silica gel (petroleum ether/ethyl acetate = 50:1−20:1). ^{1}H NMR (600 MHz, $CDCl_3$) δ 2.40 (s, 3H), 7.37−7.40 (m, 1H), 7.46 (d, J = 7.8 Hz, 1H), 7.48−7.52 (m, 2H), 7.63−7.66 (m, 1H), 7.76 (d, J = 7.8 Hz, 1H), 7.78 (s, 1H), 7.95−7.98 (m, 2H); ^{13}C NMR (150 MHz, $CDCl_3$) δ 21.18, 127.15, 128.87, 128.95, 129.83, 130.13, 132.94, 132.97, 134.80, 135.71, 138.95, 194.67, 194.81. HRMS (ESI) m/z $[M + H]^+$ calcd for $C_{15}H_{13}O_2$ 225.0910, found 225.0916.

*4.2.6. 1-Phenyl-2-(o-tolyl)ethane-1,2-dione (**2f**).* Yellow soild (54.7 mg, 81% yield, from **1**, R^1 = CH_3, R^2 = H),

https://doi.org/10.1021/acsomega.1c06017
ACS Omega 2022, 7, 1380−1394

(51.2 mg, 76% yield, from **1**, R^1 = H, R^2 = CH_3), purified by column chromatography on silica gel (petroleum ether/ethyl acetate = 50:1−20:1). ^{1}H NMR (600 MHz, $CDCl_3$) δ 2.70 (s, 3H), 7.24−7.27 (m, 1H), 7.34 (d, J = 7.2 Hz, 1H), 7.46−7.52 (m, 3H), 7.63−7.66 (m, 2H), 7.96−7.98 (m, 2H); ^{13}C NMR (150 MHz, $CDCl_3$) δ 21.85, 125.98, 128.97, 129.87, 131.72, 132.53, 133.00, 133.06, 133.75, 134.66, 141.31, 194.81, 196.76. HRMS (ESI) m/z [M + H]$^+$ calcd for $C_{15}H_{13}O_2$ 225.0910, found 225.0917.

*4.2.7. 1-(3,5-Dimethylphenyl)-2-phenylethane-1,2-dione (**2g**).* Yellow solid (50.9 mg, 71% yield), purified by column chromatography on silica gel (petroleum ether/ethyl acetate = 50:1−20:1). ^{1}H NMR (600 MHz, $CDCl_3$) δ 2.36 (s, 6H), 7.29 (s, 1H), 7.49−7.53 (m, 2H), 7.57 (s, 2H), 7.64−7.67 (m, 1H), 7.95−7.98 (m, 2H); ^{13}C NMR (150 MHz, $CDCl_3$) δ 21.11, 127.58, 128.97, 129.90, 133.02, 133.07, 134.78, 136.72, 138.85, 194.83, 195.11. HRMS (ESI) m/z [M + H]$^+$ calcd for $C_{16}H_{15}O_2$ 239.1067, found 239.1073.

*4.2.8. 1-([1,1′-Biphenyl]-4-yl)-2-phenylethane-1,2-dione (**2h**).* Yellowish solid (68.8 mg, 80% yield), purified by column chromatography on silica gel (petroleum ether/ethyl acetate = 50:1−20:1). ^{1}H NMR (600 MHz, $CDCl_3$) δ 7.38−7.41 (m, 1H), 7.44−7.47 (m, 2H), 7.49−7.52 (m, 2H), 7.59-7.62 (m, 2H), 7.63−7.66 (m, 1H), 7.70-7.72 (m, 2H), 7.99−8.01 (m, 2H), 8.03−8.05 (m, 2H); ^{13}C NMR (150 MHz, $CDCl_3$) δ 127.28, 127.58, 128.59, 128.98, 129.88, 130.42, 131.62, 132.97, 134.83, 139.38, 147.52, 194.09, 194.51. HRMS (ESI) m/z [M + H]$^+$ calcd for $C_{20}H_{15}O_2$ 287.1067, found 287.1069.

*4.2.9. 1-(4-Chlorophenyl)-2-phenylethane-1,2-dione (**2i**).* Yellow solid (55.4 mg, 75% yield, from **1**, R^1 = Cl, R^2 = H), (57.7 mg, 79% yield, from **1**, R^1 = H, R^2 = Cl), purified by column chromatography on silica gel (petroleum ether/ethyl acetate = 50:1−20:1). ^{1}H NMR (600 MHz, $CDCl_3$) δ 7.47−7.53 (m, 4H), 7.65−7.68 (m, 1H), 7.91−7.94 (m, 2H), 7.96 (dd, J_1 = 8.4 Hz, J_2 = 1.2 Hz, 2H); ^{13}C NMR (150 MHz, $CDCl_3$) δ 129.04, 129.41, 129.90, 131.18, 131.30, 132.72, 135.03, 141.55, 193.04, 193.85. HRMS (ESI) m/z [M + H]$^+$ calcd for $C_{14}H_{10}ClO_2$ 245.0364, found 245.0366.

*4.2.10. 1-(4-Bromophenyl)-2-phenylethane-1,2-dione (**2j**).* Yellow solid (61.7 mg, 71% yield, from **1**, R^1 = Br, R^2 = H), (62.5 mg, 72% yield, from **1**, R^1 = H, R^2 = Br), purified by column chromatography on silica gel (petroleum ether/ethyl acetate = 50:1-20:1). 1H NMR (600 MHz, $CDCl_3$) δ 7.50−7.53 (m, 2H), 7.64−7.68 (m, 3H), 7.82−7.86 (m, 2H), 7.96 (dd, J_1 = 8.4 Hz, J_2 = 1.2 Hz, 2H); ^{13}C NMR (150 MHz, $CDCl_3$) δ 129.04, 129.90, 130.45, 131.19, 131.68, 132.38, 132.71, 135.03, 193.23, 193.80. HRMS (ESI) m/z [M + H]$^+$ calcd for $C_{14}H_{10}BrO_2$ 288.9859, found 288.9862.

*4.2.11. 1-(4-Fluorophenyl)-2-phenylethane-1,2-dione (**2k**).*[95] Yellow solid (36.7 mg, 54% yield, from **1**, R^1 = F, R^2 = H), (42.5 mg, 62% yield, from **1**, R^1 = H, R^2 = F), purified by column chromatography on silica gel (petroleum ether/ethyl acetate = 50:1-20:1). ^{1}H NMR (600 MHz, $CDCl_3$) δ 7.17−7.21 (m, 2H), 7.50−7.54 (m, 2H), 7.65−7.69 (m, 1H), 7.96−7.98 (m, 2H), 8.00−8.04 (m, 2H); ^{13}C NMR (150 MHz, $CDCl_3$) δ 116.37 ($J_{C\text{-}F}$ = 21.6 Hz), 129.04, 129.47 ($J_{C\text{-}F}$ = 2.4 Hz), 129.91, 132.71 ($J_{C\text{-}F}$ = 9.9 Hz), 132.80, 134.99, 166.76 ($J_{C\text{-}F}$ = 256.8 Hz), 192.72, 194.06. HRMS (ESI) m/z [M + H]$^+$ calcd for $C_{14}H_{10}FO_2$ 229.0659, found 229.0661.

*4.2.12. 1-(4-Acetylphenyl)-2-phenylethane-1,2-dione (**2l**).* Yellow solid (36.1 mg, 48% yield), purified by column chromatography on silica gel (petroleum ether/ethyl acetate = 20:1−10:1). ^{1}H NMR (600 MHz, $CDCl_3$) δ 2.66 (s, 3H), 7.52−7.55 (m, 2H), 7.67−7.70 (m, 1H), 7.97−7.99 (m, 2H), 8.07 (brs, 4H); ^{13}C NMR (150 MHz, $CDCl_3$) δ 26.91, 128.68, 129.10, 129.94, 130.07, 132.65, 135.15, 135.94, 141.29, 193.59, 193.74, 197,21. HRMS (ESI) m/z [M + H]$^+$ calcd for $C_{16}H_{13}O_3$ 253.0859, found 253.0863.

*4.2.13. 1-(3-Chlorophenyl)-2-phenylethane-1,2-dione (**2m**).* Yellow solid (51.4 mg, 70% yield, from **1**, R^1 = Cl, R^2 = H), (44.9 mg, 61% yield, from **1**, R^1 = H, R^2 = Cl), purified by column chromatography on silica gel (petroleum ether/ethyl acetate = 50:1-20:1). ^{1}H NMR (600 MHz, $CDCl_3$) δ 7.44−7.47 (m, 1H), 7.51−7.54 (m, 2H), 7.61−7.64 (m, 1H), 7.66−7.69 (m, 1H), 7.83−7.85 (m, 1H), 7.96−7.98 (m, 3H); ^{13}C NMR (150 MHz, $CDCl_3$) δ 128.09, 129.08, 129.53, 129.94, 130.34, 132.63, 134.46, 134.76, 135.12, 135.39, 192.94, 193.59. HRMS (ESI) m/z [M + H]$^+$ calcd for $C_{14}H_{10}ClO_2$ 245.0364, found 245.0368.

*4.2.14. 1-(2-Chlorophenyl)-2-phenylethane-1,2-dione (**2n**).* Yellow oil (34.2 mg, 47% yield, from **1**, R^1 = Cl, R^2 = H), (42.3 mg, 58% yield, from **1**, R^1 = H, R^2 = Cl), purified by column chromatography on silica gel (petroleum ether/ethyl acetate = 50:1-20:1). ^{1}H NMR (600 MHz, $CDCl_3$) δ 7.42−7.45 (m, 2H), 7.52−7.56 (m, 3H), 7.64−7.68 (m, 1H), 7.89−7.92 (m, 1H), 8.02−8.05 (m, 2H); ^{13}C NMR (150 MHz, $CDCl_3$) δ 127.35, 128.87, 130.19, 130.49, 132.09, 132.41, 133.83, 133.97, 134.51, 134.57, 192.05, 193.67. HRMS (ESI) m/z [M + H]$^+$ calcd for $C_{14}H_{10}ClO_2$ 245.0364, found 245.0367.

*4.2.15. 1-(Naphthalen-1-yl)-2-phenylethane-1,2-dione (**2o**).* Yellow solid (47.5 mg, 61% yield), purified by column chromatography on silica gel (petroleum ether/ethyl acetate = 50:1−20:1). ^{1}H NMR (600 MHz, $CDCl_3$) δ 7.47−7.53 (m, 3H), 7.61−7.67 (m, 2H), 7.73−7.76 (m, 1H), 7.91 (dd, J_1 = 7.2 Hz, J_2 = 1.2 Hz, 1H), 7.94 (d, J = 7.8 Hz, 1H), 8.02-8.04 (m, 2H), 8.12 (d, J = 7.8 Hz, 1H), 9.31 (d, J = 9.0 Hz, 1H); ^{13}C NMR (150 MHz, $CDCl_3$) δ 124.41, 125.94, 127.11, 128.62, 128.78, 129.03, 129.45, 130.02, 130.94, 133.36, 134.08, 134.73, 135.06, 135.96, 194.58, 197.16. HRMS (ESI) m/z [M + H]$^+$ calcd for $C_{18}H_{13}O_2$ 261.0910, found 261.0916.

*4.2.16. 1-(Naphthalen-2-yl)-2-phenylethane-1,2-dione (**2p**).* Yellow solid (55.8 mg, 71% yield), purified by column chromatography on silica gel (petroleum ether/ethyl acetate = 50:1−20:1). ^{1}H NMR (600 MHz, $CDCl_3$) δ 7.51−7.57 (m, 3H), 7.62−7.68 (m, 2H), 7.88−7.92 (m, 2H), 7.96 (d, J = 8.4 Hz, 1H), 8.02−8.04 (m, 2H), 8.10 (dd, J_1 = 9.0 Hz, J_2 = 1.8 Hz, 1H), 8.41 (s, 1H); ^{13}C NMR (150 MHz, $CDCl_3$) δ 123.64, 127.16, 127.94, 129.03, 129.16, 129.53, 129.92, 129.98, 130.31, 132.33, 133.12, 133.53, 134.89, 136.38, 194.64. HRMS (ESI) m/z [M + H]$^+$ calcd for $C_{18}H_{13}O_2$ 261.0910, found 261.0918.

*4.2.17. 1-(Furan-3-yl)-2-phenylethane-1,2-dione (**2q**).* Yellow oil (29.4 mg, 49% yield), purified by column chromatography on silica gel (petroleum ether/ethyl acetate = 50:1−20:1). ^{1}H NMR (600 MHz, $CDCl_3$) δ 6.94 (dd, J_1 = 1.8 Hz, J_2 = 0.6 Hz, 1H), 7.50−7.54 (m, 3H), 7.64−7.68 (m, 1H), 8.03−8.06 (m, 2H), 8.19−8.20 (m, 1H); ^{13}C NMR (150 MHz, $CDCl_3$) δ 108.59, 123.98, 128.87, 130.33, 132.49, 134.76, 144.60, 151.33, 187.01, 191.84. HRMS (ESI) m/z [M + H]$^+$ calcd for $C_{12}H_9O_3$ 201.0546, found 201.0552.

*4.2.18. 1-Phenyl-2-(thiophen-3-yl)ethane-1,2-dione (**2r**).* Yellow oil (58.4 mg, 90% yield), purified by column chromatography on silica gel (petroleum ether/ethyl acetate = 50:1−20:1). ^{1}H NMR (600 MHz, $CDCl_3$) δ 7.39−7.41 (m, 1H), 7.49−7.52 (m, 2H), 7.63−7.67 (m, 2H), 7.99−8.02 (m,

https://doi.org/10.1021/acsomega.1c06017
ACS Omega 2022, 7, 1380−1394

2H), 8.21−8.22 (m, 1H); ^{13}C NMR (150 MHz, $CDCl_3$) δ 127.04, 127.18, 128.88, 130.05, 132.62, 134.76, 136.98, 137.97, 187.24, 193.21. HRMS (ESI) m/z [M + H]$^+$ calcd for $C_{12}H_9O_2S$ 217.0318, found 217.0324.

*4.2.19. Methyl 4-(2-oxo-2-phenylacetyl)benzoate (**2s**).* Yellow solid (50.4 mg, 63% yield), purified by column chromatography on silica gel (petroleum ether/ethyl acetate = 50:1−20:1). ^{1}H NMR (600 MHz, $CDCl_3$) δ 3.96 (s, 3H), 7.51−7.55 (m, 2H), 7.66−7.70 (m, 1H), 7.97−7.99 (m, 2H), 8.04 (d, J = 8.4 Hz, 2H), 8.15−8.18 (m, 2H); ^{13}C NMR (150 MHz, $CDCl_3$) δ 52.57, 129.08, 129.73, 129.92, 130.05, 132.64, 135.11, 135.27, 136.00, 165.83, 193.63, 193.75. HRMS (ESI) m/z [M + H]$^+$ calcd for $C_{16}H_{13}O_4$ 269.0808, found 269.0809.

*4.2.20. 1-(4-Nitrophenyl)-2-phenylethane-1,2-dione (**2t**).* Yellow solid (28.4 mg, 37% yield), purified by column chromatography on silica gel (petroleum ether/ethyl acetate = 50:1−20:1). ^{1}H NMR (600 MHz, $CDCl_3$) δ 7.54−7.57 (m, 2H), 7.70−7.73 (m, 1H), 7.98−8.00 (m, 2H), 8.18 (d, J = 9.0 Hz, 2H), 8.36 (d, J = 8.4 Hz, 2H); ^{13}C NMR (150 MHz, $CDCl_3$) δ 124.13, 129.24, 130.06, 130.97, 132.38, 135.47, 137.31, 151.16, 192.08, 192.86. HRMS (ESI) m/z [M + Na]$^+$ calcd for $C_{14}H_9NO_4Na$ 278.0424, found 278.0428.

*4.2.21. 2,3-Diphenylquinoxaline (**4aa**).* White solid (77.6 mg, 92% yield), purified by column chromatography on silica gel (petroleum ether/ethyl acetate = 50:1−20:1). ^{1}H NMR (600 MHz, $CDCl_3$) δ 7.29−7.36 (m, 6H), 7.50−7.53 (m, 4H), 7.71−7.75 (m, 2H), 8.15−8.19 (m, 2H); ^{13}C NMR (150 MHz, $CDCl_3$) δ 128.17, 128.70, 129.10, 129.75, 129.85, 138.98, 141.13, 153.35. HRMS (ESI) m/z [M + H]$^+$ calcd for $C_{20}H_{15}N_2$ 283.1230, found 283.1229.

*4.2.22. 2-Phenyl-3-(p-tolyl)quinoxaline (**4ba**).* White solid (78.1 mg, 88% yield), purified by column chromatography on silica gel (petroleum ether/ethyl acetate = 50:1−20:1). ^{1}H NMR (600 MHz, $CDCl_3$) δ 2.34 (s, 3H), 7.12 (d, J = 7.8 Hz, 2H), 7.31−7.37 (m, 3H), 7.41 (d, J = 7.8 Hz, 2H), 7.52−7.55 (m, 2H), 7.71−7.75 (m, 2H), 8.14−8.17 (m, 2H); ^{13}C NMR (150 MHz, $CDCl_3$) δ 21.25, 128.19, 128.66, 128.91, 129.08, 129.67, 129.73, 129.78, 136.11, 138.76, 139.23, 141.02, 141.21, 153.40. HRMS (ESI) m/z [M + H]$^+$ calcd for $C_{21}H_{17}N_2$ 297.1386, found 297.1387.

*4.2.23. 2-(4-Methoxyphenyl)-3-phenylquinoxaline (**4ca**).* Yellowish solid (76.2 mg, 81% yield), purified by column chromatography on silica gel (petroleum ether/ethyl acetate = 50:1−20:1). ^{1}H NMR (600 MHz, $CDCl_3$) δ 3.77 (s, 3H), 6.82−6.85 (m, 2H), 7.31−7.37 (m, 3H), 7.45−7.49 (m, 2H), 7.52−7.55 (m, 2H), 7.68−7.73 (m, 2H), 8.12-8.15 (m, 2H); ^{13}C NMR (150 MHz, $CDCl_3$) δ 55.14, 113.60, 128.19, 128.62, 128.92, 129.01, 129.48, 129.63, 129.73, 131.26, 139.30, 140.86, 141.17, 152.89, 153.27, 160.10. HRMS (ESI) m/z [M + H]$^+$ calcd for $C_{21}H_{17}N_2O$ 313.1335, found 313.1334.

*4.2.24. 2-([1,1′-Biphenyl]-4-yl)-3-phenylquinoxaline (**4ha**).* White solid (80.6 mg, 75% yield), purified by column chromatography on silica gel (petroleum ether/ethyl acetate = 50:1−20:1). ^{1}H NMR (600 MHz, $CDCl_3$) δ 7.32−7.39 (m, 4H), 7.40−7.44 (m, 2H), 7.55−7.62 (m, 8H), 7.73−7.77 (m, 2H), 8.16−8.20 (m, 2H); ^{13}C NMR (150 MHz, $CDCl_3$) δ 126.88, 127.02, 127.56, 128.31, 128.76, 128.81, 129.14, 129.81, 129.90, 129.92, 130.28, 137.90, 139.08, 140.29, 141.15, 141.24, 141.43, 152.99, 153.39. HRMS (ESI) m/z [M + H]$^+$ calcd for $C_{26}H_{19}N_2$ 359.1543, found 359.1544.

*4.2.25. 2-(4-Chlorophenyl)-3-phenylquinoxaline (**4ia**).* White solid (70.3 mg, 74% yield), purified by column chromatography on silica gel (petroleum ether/ethyl acetate = 50:1−20:1). ^{1}H NMR (600 MHz, $CDCl_3$) δ 7.28−7.31 (m, 2H), 7.33−7.39 (m, 3H), 7.45−7.48 (m, 2H), 7.49−7.52 (m, 2H), 7.74−7.78 (m, 2H), 8.13−8.17 (m, 2H); ^{13}C NMR (150 MHz, $CDCl_3$) δ 128.40, 128.46, 128.94, 129.09, 129.16, 129.73, 130.07, 130.14, 131.19, 135.05, 137.43, 138.76, 141.11, 141.21, 152.07, 153.17. HRMS (ESI) m/z [M + H]$^+$ calcd for $C_{20}H_{14}ClN_2$ 317.0840, found 317.0843.

*4.2.26. 2-(4-Bromophenyl)-3-phenylquinoxaline (**4ja**).* White solid (65.7 mg, 61% yield), purified by column chromatography on silica gel (petroleum ether/ethyl acetate = 50:1−20:1). ^{1}H NMR (600 MHz, $CDCl_3$) δ 7.35−7.42 (m, 5H), 7.46−7.48 (m, 2H), 7.50−7.52 (m, 2H), 7.76−7.79 (m, 2H), 8.15−8.19 (m, 2H); ^{13}C NMR (150 MHz, $CDCl_3$) δ 123.45, 128.46, 128.99, 129.15, 129.22, 129.76, 130.12, 130.20, 131.45, 131.47, 137.95, 138.78, 141.18, 141.26, 152.15, 153.19. HRMS (ESI) m/z [M + H]$^+$ calcd for $C_{20}H_{14}{}^{79}BrN_2$ 361.0335, found 361.0321; $C_{20}H_{14}{}^{81}BrN_2$ 363.0314, found 363.0302.

*4.2.27. 2-(4-Fluorophenyl)-3-phenylquinoxaline (**4ka**).*[95] White solid (49.1 mg, 54% yield), purified by column chromatography on silica gel (petroleum ether/ethyl acetate = 50:1−20:1). ^{1}H NMR (600 MHz, $CDCl_3$) δ 7.00−7.04 (m, 2H), 7.33−7.38 (m, 3H), 7.49−7.53 (m, 4H), 7.75−7.79 (m, 2H), 8.14-8.18 (m, 2H); ^{13}C NMR (150 MHz, $CDCl_3$) δ 115.33 ($J_{C\text{-}F}$ = 21.5Hz), 128.38, 128.90, 129.09, 129.19, 129.73, 130.04, 130.05, 131.79 ($J_{C\text{-}F}$ = 8.3Hz), 135.07 ($J_{C\text{-}F}$ = 3.2Hz), 138.92, 141.15, 141.20, 152.29, 153.28, 163.14 ($J_{C\text{-}F}$ = 248.1 Hz). HRMS (ESI) m/z [M + H]$^+$ calcd for $C_{20}H_{14}FN_2$ 301.1136, found 301.1125.

*4.2.28. 2-(Naphthalen-2-yl)-3-phenylquinoxaline (**4pa**).* White solid (72.1 mg, 72% yield), purified by column chromatography on silica gel (petroleum ether/ethyl acetate = 50:1−20:1). ^{1}H NMR (600 MHz, $CDCl_3$) δ 7.27−7.30 (m, 2H), 7.31−7.35 (m, 1H), 7.43−7.50 (m, 2H), 7.51 (dd, J_1 = 8.4 Hz, J_2 = 1.8 Hz, 1H), 7.53−7.56 (m, 2H), 7.73 (d, J = 8.4 Hz, 1H), 7.74−7.78 (m, 2H), 7.79 (d, J = 7.8 Hz, 2H), 8.14 (s, 1H), 8.18−8.22 (m, 2H); ^{13}C NMR (150 MHz, $CDCl_3$) δ 126.22, 126.77, 127.01, 127.59, 127.62, 128.31, 128.58, 128.81, 129.16, 129.18, 129.77, 129.80, 129.95, 133.10, 133.18, 136.48, 139.04, 141.19, 141.29, 153.22, 153.53. HRMS (ESI) m/z [M + H]$^+$ calcd for $C_{24}H_{17}N_2$ 333.1386, found 333.1387.

*4.2.29. 2-Phenyl-3-(thiophen-3-yl)quinoxaline (**4ra**).* White solid (63.4 mg, 73% yield), purified by column chromatography on silica gel (petroleum ether/ethyl acetate = 50:1−20:1). ^{1}H NMR (600 MHz, $CDCl_3$) δ 7.21−7.26 (m, 2H), 7.41−7.44 (m, 4H), 7.55−7.59 (m, 2H), 7.71−7.76 (m, 2H), 8.11−8.16 (m, 2H); ^{13}C NMR (150 MHz, $CDCl_3$) δ 125.18, 127.46, 128.38, 128.65, 128.94, 128.95, 129.04, 129.37, 129.68, 129.89, 139.23, 140.05, 140.77, 141.17, 148.43, 153.31. HRMS (ESI) m/z [M + H]$^+$ calcd for $C_{18}H_{13}N_2S$ 289.0794, found 289.0793.

*4.2.30. 6-Methyl-2,3-diphenylquinoxaline (**4ab**).* White solid (72.5 mg, 82% yield), purified by column chromatography on silica gel (petroleum ether/ethyl acetate = 50:1−20:1). ^{1}H NMR (600 MHz, $CDCl_3$) δ 2.58 (s, 3H), 7.28−7.35 (m, 6H), 7.48−7.51 (m, 4H), 7.56 (d, J = 8.4 Hz, 1H), 7.94 (s, 1H), 8.05 (d, J = 8.4 Hz, 1H); ^{13}C NMR (150 MHz, $CDCl_3$) δ 21.79, 127.91, 128.10, 128.51, 128.57, 128.58, 129.73, 129.74, 132.18, 139.11, 139.59, 140.35, 141.17, 152.44, 153.19. HRMS (ESI) m/z [M + H]$^+$ calcd for $C_{21}H_{17}N_2$ 297.1386, found 297.1387.

*4.2.31. 6-Methoxy-2,3-diphenylquinoxaline (**4ac**).* White solid (76.7 mg, 82% yield), purified by column chromatography on silica gel (petroleum ether/ethyl acetate = 50:1−

https://doi.org/10.1021/acsomega.1c06017
ACS Omega 2022, 7, 1380−1394

20:1). ^{1}H NMR (600 MHz, $CDCl_3$) δ 3.95 (s, 3H), 7.28−7.35 (m, 6H), 7.40 (dd, J_1 = 9.0 Hz, J_2 = 3.0 Hz, 1H), 7.45 (d, J = 2.4 Hz, 1H), 7.48−7.52 (m, 4H), 8.04 (d, J = 8.4 Hz, 1H); ^{13}C NMR (150 MHz, $CDCl_3$) δ 55.70, 106.35, 123.23, 128.10, 128.13, 128.34, 128.55, 129.71, 130.04, 137.28, 139.11, 139.17, 142.65, 150.80, 153.22, 160.77. HRMS (ESI) m/z $[M + H]^+$ calcd for $C_{21}H_{17}N_2O$ 313.1335, found 313.1335.

*4.2.32. 6-Chloro-2,3-diphenylquinoxaline (**4ad**).* Yellowish solid (82.6 mg, 87% yield), purified by column chromatography on silica gel (petroleum ether/ethyl acetate = 50:1−20:1). ^{1}H NMR (600 MHz, $CDCl_3$) δ 7.29−7.37 (m, 6H), 7.48−7.51 (m, 4H), 7.65−7.68 (m, 1H), 8.07 (d, J = 9.0 Hz, 1H), 8.15 (d, J = 3.0 Hz, 1H); ^{13}C NMR (150 MHz, CDCl3) δ 127.97, 128.21, 128.22, 128.92, 129.01, 129.72, 129.76, 130.33, 130.83, 135.54, 138.55, 138.62, 139.60, 141.37, 153.49, 154.16. HRMS (ESI) m/z $[M + H]^+$ calcd for $C_{20}H_{14}ClN_2$ 317.0840, found 317.0842.

*4.2.33. 2,3-Diphenylquinoxaline-6-carbonitrile (**4ae**).* White solid (79.6 mg, 86% yield), purified by column chromatography on silica gel (petroleum ether/ethyl acetate = 50:1−20:1). ^{1}H NMR (600 MHz, $CDCl_3$) δ 7.33−7.36 (m, 4H), 7.38−7.42 (m, 2H), 7.51−7.55 (m, 4H), 7.85−7.88 (m, 1H), 8.23 (dd, J_1 = 9.0 Hz, J_2 = 0.6 Hz, 1H), 8.51 (s, 1H); ^{13}C NMR (150 MHz, $CDCl_3$) δ 113.06, 118.04, 128.30, 129.42, 129.52, 129.70, 129.76, 130.49, 130.62, 134.97, 137.99, 138.04, 140.08, 142.42, 155.20, 155.78. HRMS (ESI) m/z $[M + H]^+$ calcd for $C_{21}H_{14}N_3$ 308.1182, found 308.1183.

*4.2.34. Methyl 2,3-diphenylquinoxaline-6-carboxylate (**4af**).* White solid (79.7 mg, 78% yield), purified by column chromatography on silica gel (petroleum ether/ethyl acetate = 50:1−20:1). ^{1}H NMR (600 MHz, $CDCl_3$) δ 4.00 (s, 3H), 7.31−7.35 (m, 4H), 7.35−7.39 (m, 2H), 7.52−7.55 (m, 4H), 8.18 (d, J = 9.0 Hz, 1H), 8.33 (dd, J_1 = 8.7 Hz, J_2 = 2.4 Hz, 1H), 8.88 (d, J = 2.4 Hz, 1H); ^{13}C NMR (150 MHz, $CDCl_3$) δ 52.48, 128.22, 129.03, 129.16, 129.30, 129.34, 129.74, 129.78, 131.08, 131.80, 138.51, 140.28, 143.04, 154.29, 155.00, 166.20. HRMS (ESI) m/z $[M + H]^+$ calcd for $C_{22}H_{17}N_2O_2$ 341.1285, found 341.1286.

*4.2.35. 2,3-Diphenylbenzo[g]quinoxaline (**4ag**).* Yellow solid (85.2 mg, 85% yield), purified by column chromatography on silica gel (petroleum ether/ethyl acetate = 50:1−20:1). ^{1}H NMR (600 MHz, $CDCl_3$) δ 7.30−7.37 (m, 6H), 7.48−7.51 (m, 2H), 7.54−7.56 (m, 4H), 8.03−8.06 (m, 2H), 8.70 (s, 2H); ^{13}C NMR (150 MHz, $CDCl_3$) δ 126.58, 127.42, 128.14, 128.40, 128.89, 129.75, 133.92, 137.82, 139.04, 154.01. HRMS (ESI) m/z $[M + H]^+$ calcd for $C_{24}H_{17}N_2$ 333.1386, found 333.1388.

*4.2.36. 5-Methyl-2,3-diphenylquinoxaline (**4ah**).* Yellow solid (73.3 mg, 82% yield), purified by column chromatography on silica gel (petroleum ether/ethyl acetate = 50:1−20:1). ^{1}H NMR (600 MHz, $CDCl_3$) δ 2.84 (s, 3H), 7.28−7.36 (m, 6H), 7.51−7.54 (m, 2H), 7.55−7.58 (m, 3H), 7.60−7.63 (m, 1H), 7.99 (dd, J_1 = 8.4 Hz, J_2 = 0.6 Hz, 1H); ^{13}C NMR (150 MHz, $CDCl_3$) δ 17.07, 126.89, 128.03, 128.22, 128.61, 129.61, 129.72, 129.75, 130.08, 137.54, 139.30, 139.35, 140.32, 141.09, 151.69, 152.74. HRMS (ESI) m/z $[M + H]^+$ calcd for $C_{21}H_{17}N_2$ 297.1386, found 297.1386.

*4.2.37. 2,3-Bis(4-methoxyphenyl)-5-methylquinoxaline (**4uh**).* Yellowish solid (86.9 mg, 81% yield), purified by column chromatography on silica gel (petroleum ether/ethyl acetate = 50:1−20:1). ^{1}H NMR (600 MHz, $CDCl_3$) δ 2.82 (s, 3H), 3.79 (s, 3H), 3.80 (s, 3H), 6.83−6.88 (m, 4H), 7.48−7.52 (m, 3H), 7.52−7.58 (m, 3H), 7.94 (dd, J_1 = 8.1 Hz, J_2 = 1.2 Hz, 1H); ^{13}C NMR (150 MHz, $CDCl_3$) δ 17.01, 55.16, 55.19, 113.50, 113.69, 126.65, 129.12, 129.32, 131.09, 131.39, 131.93, 137.21, 140.07, 140.85, 151.18, 152.20, 159.99, 160.02. HRMS (ESI) m/z $[M + H]^+$ calcd for $C_{23}H_{21}N_2O_2$ 357.1598, found 357.1594.

4.3. Cell Viability Assay. The MTT assay was utilized to examine the cytotoxic effects of quinoxalines on both HEK-293T-ACE2^h cells and four human cancer cell lines mentioned below. HEK-293T-ACE2^h cells were constructed by Sino Biological (Beijing, China) and cultured in Dulbecco's modified Eagle's medium (DMEM) supplemented with 10% fetal bovine serum and the antibiotics of penicillin (50 U/mL), streptomycin (50 μg/mL, Invitrogen, Paisley, Scotland, U.K.), and hygromycin (100 μg/mL) at 37 °C in a humidified atmosphere of 5% CO_2. HEK-293T-ACE2^h cells were seeded into a 96-well plate at a density of 1 × 10^4 cells per well and then treated with different concentrations of compounds for 4 h to measure the maximum nontoxic concentration (CC_0) of quinoxalines. The CC_0 values of quinoxalines for 4 h were determined as the highest tested concentration at which cell viability was 100%. The TC_{50} value was determined as the concentration that caused 50% cells' death for 4 h quinoxalines' treatment. The human breast cancer cell lines (MCF-7 and T47D) and human lung carcinoma cell line (A549) were purchased from the American Type Culture Collection (ATCC, Rockville, MD), and cultivated in DMEM containing 10% fetal bovine serum (FBS) and 1% penicillin−streptomycin. The triple-negative breast cancer cell line (MDA-MB-231) was provided by Cell Bank of Chinese Academy of Sciences (Shanghai, China) and cultured in RPMI 1640 medium supplemented with 10% FBS and 1% penicillin−streptomycin. First, cancer cells were seeded in 96-well plates at a density of 2 × 10^3−4 × 10^3 cells per well and then incubated for 24 h at 37 °C with 5% CO_2. Subsequently, various concentrations (0−40 μM) of quinoxalines and berberine (as the positive control alkaloid) were added to each well. After further incubation for 72 h, 10 μL of MTT (5 mg/mL) was administered to each well and incubated for another 4 h. DMSO (100 μL) was then added to each well, and the plate was agitated for 10 min to dissolve the formazan completely. Finally, the absorbance value of each well was determined by a microplate reader at 570 nm. The IC_{50} values were calculated with the SPSS 20.0 software. All of the data were obtained in triplicate and presented as mean ± SD.

4.4. Detection of SARS-CoV-2 Spike Pseudovirus Entry into HEK-293T-ACE2^h Cells. In HEK-293T cells, pNL4-3.Luc.R-E- plasmid (from the NIH AIDS repository) and pcDNA3.1-SARS-CoV-2-Spike-Myc plasmid (from Beyotime, Shanghai, China) were utilized to produce SARS-CoV-2 spike pseudotyped viruses according to the published protocol.[63] The infectious competency of 30 μL generated pseudovirus was quantified in hexaplicate to be equivalent to that of 8.05 ± 0.39 × 10^7 copies of SARS-CoV-2 pseudovirus (10^{10} copies/mL, PSV001) from Sino Biological by a viral infection equation: $Y = 197.06X - 87.679$, $R^2 = 0.9997$. HEK-293T-ACE2^h cells (1 × 10^4 in 100 μL DMEM) were seeded in 96-well plates and cultured for 24 h. The culture medium was then replaced with 100 μL of compound-containing DMEM for a 2 h incubation at 37 °C. Following that, 30 μL of produced pseudovirus (MOI = 100 virus particles/cell), 20 μL of media, and 50 μL of twofold concentration of compounds were simultaneously supplemented to each well for another 2 h incubation at 37 °C. After removing the inoculum, the cells

https://doi.org/10.1021/acsomega.1c06017
ACS Omega 2022, 7, 1380−1394

were overlaid with 100 μL of fresh DMEM and continuously incubated at 37 °C for 48 h. The culture media were discarded, and the cells were washed with PBS once. The plate was then agitated for 10 min after 100 μL of cell lysate solution was supplemented to each well. The cell lysate was then transferred to an opaque 96-well white solid plate, and 100 μL of luminescence solution was filled into each well according to instructions of the Firefly Luciferase Reporter Gene Assay Kit (Beyotime, China). Immediately, the luciferase luminescence in each well was determined at 578 nm by a microplate reader (SpectraMax iD5 Multi-Mode Microplate Reader, Molecular Devices). The control group was HEK-293T-ACE2^{h} cells infected only with SARS-CoV-2 spike pseudovirus, and the luciferase luminescence value was set as 100% for the control group. The luminescence values of compound-treated groups were normalized according to the control group.[64] The inhibitory activity of the compounds tested against pseudovirus entry was presented as an IC_{50} value, which is defined as the concentration that prevents 50% of the pseudovirus from entering the target cell. GraphPad Prism 8.0 software (La Jolla, CA) was used to compute the IC_{50} values. All of the data came from three separate experiments.

4.5. Biolayer Interferometry (BLI) Binding Assay. Biolayer interferometry was used to examine the binding kinetics of compounds with the proteins of recombinant histidine-tagged SARS-CoV-2 spike RBD and recombinant histidine-tagged human ACE2 (Sino Biological, Beijing, China) by an Octet system (Octet RED96, ForteBio).[65,66] A protein-loading program of the instrument immobilized either histidine-tagged SARS-CoV-2 spike RBD protein (25 g/mL aqueous solution) or histidine-tagged human ACE2 protein (25 g/mL aqueous solution) on nickel charged nitrilotriacetic acid (Ni-NTA) biosensors (Fortebi). Each compound's stock solution (10 mM in DMSO) was serially diluted with PBS to a final DMSO concentration of 1.0%. Before data acquisition, both protein-immobilized and empty biosensors were equilibrated in PBS for 10 min at room temperature and all experiments were carried out at 30 °C. The protein-coated and uncoated biosensors were both dipped in wells containing serially diluted samples. By dipping a protein-immobilized biosensor in the blank buffer, the background signal was subtracted from all samples. Empty biosensors were also dipped in serially diluted samples for reference subtraction under the same conditions. The subtracted sensorgrams were then fitted to a 1:1 binding model with Octet Data Analysis Software v11.1 (ForteBio), and the resulting equilibrium dissociation constant (K_D) values were calculated.

4.6. Molecular Docking Study. CDOCKER of Discovery Studio software was utilized to conduct molecular docking analysis on the structure of proteins of spike RBD from SARS-CoV-2 (PDB ID: 6M0J) and human ACE2 bound with its inhibitor (PDB ID: 1R4L), respectively. The active contact sites for compounds were determined to be Tyr449, Gln493, Gln498, Thr500, Asn501, Gly502, and Tyr505 of the spike RBD according to the reported literature.[67,68] A docking pocket was produced based on the position of the ACE2 inhibitor.[69] Discovery Studio software was utilized to analyze the binding modes.

4.7. Statistical analysis. Statistical comparisons were calculated by Student's t-test analysis, and $p < 0.05$ was regarded as statistically significant.

■ ASSOCIATED CONTENT

Supporting Information

The Supporting Information is available free of charge at https://pubs.acs.org/doi/10.1021/acsomega.1c06017.

Quinoxalines **4aa**−**4ta** with calculated binding energy with both human ACE2 and SARS-CoV-2 spike RBD proteins by molecular docking study, ^{1}H-NMR and ^{13}C-NMR spectra of products **2** and **4**, and HRMS spectra of products **2** and **4** (PDF)

■ AUTHOR INFORMATION

Corresponding Authors

Yanzhong Li − *School of Chemistry and Molecular Engineering, East China Normal University, Shanghai 200241, China;* orcid.org/0000-0002-2898-3075; Email: yzli@chem.ecnu.edu.cn

Li-Ping Bai − *State Key Laboratory of Quality Research in Chinese Medicine, Macau Institute for Applied Research in Medicine and Health, Guangdong-Hong Kong-Macao Joint Laboratory of Respiratory Infectious Disease, Macau University of Science and Technology, Taipa 999078 Macau, People's Republic of China;* orcid.org/0000-0002-2806-6883; Email: lpbai@must.edu.mo

Authors

Lingkai Kong − *State Key Laboratory of Quality Research in Chinese Medicine, Macau Institute for Applied Research in Medicine and Health, Guangdong-Hong Kong-Macao Joint Laboratory of Respiratory Infectious Disease, Macau University of Science and Technology, Taipa 999078 Macau, People's Republic of China; School of Chemistry and Chemical Engineering, Linyi University, Linyi, Shandong 276000, People's Republic of China*

Jieru Meng − *State Key Laboratory of Quality Research in Chinese Medicine, Macau Institute for Applied Research in Medicine and Health, Guangdong-Hong Kong-Macao Joint Laboratory of Respiratory Infectious Disease, Macau University of Science and Technology, Taipa 999078 Macau, People's Republic of China*

Wenyue Tian − *State Key Laboratory of Quality Research in Chinese Medicine, Macau Institute for Applied Research in Medicine and Health, Guangdong-Hong Kong-Macao Joint Laboratory of Respiratory Infectious Disease, Macau University of Science and Technology, Taipa 999078 Macau, People's Republic of China*

Jiazheng Liu − *State Key Laboratory of Quality Research in Chinese Medicine, Macau Institute for Applied Research in Medicine and Health, Guangdong-Hong Kong-Macao Joint Laboratory of Respiratory Infectious Disease, Macau University of Science and Technology, Taipa 999078 Macau, People's Republic of China*

Xueping Hu − *School of Chemistry and Chemical Engineering, Linyi University, Linyi, Shandong 276000, People's Republic of China*

Zhi-Hong Jiang − *State Key Laboratory of Quality Research in Chinese Medicine, Macau Institute for Applied Research in Medicine and Health, Guangdong-Hong Kong-Macao Joint Laboratory of Respiratory Infectious Disease, Macau University of Science and Technology, Taipa 999078 Macau, People's Republic of China;* orcid.org/0000-0002-7956-2481

https://doi.org/10.1021/acsomega.1c06017
ACS Omega 2022, 7, 1380−1394

Wei Zhang − *State Key Laboratory of Quality Research in Chinese Medicine, Macau Institute for Applied Research in Medicine and Health, Guangdong-Hong Kong-Macao Joint Laboratory of Respiratory Infectious Disease, Macau University of Science and Technology, Taipa 999078 Macau, People's Republic of China;* orcid.org/0000-0002-1620-6332

Complete contact information is available at: https://pubs.acs.org/10.1021/acsomega.1c06017

Notes

The authors declare no competing financial interest.

■ ACKNOWLEDGMENTS

This research was funded by The Science and Technology Development Fund, Macau SAR (File no. 0065/2020/A2, 0074/2019/AMJ, 0023/2019/AKP, and 0002/2019/APD) and the Natural Science Foundation of Shandong Province (ZR2020QB013). This work was also supported by the Emergency Key Program of Guangzhou Laboratory (grant no. EKPG21-06). The authors also thank the Department of Science and Technology of Guangdong Province for the support of Guangdong-Hong Kong-Macao Joint Laboratory of Respiratory Infectious Disease.

■ REFERENCES

(1) Maurya, R.; Singh, R.; Deepak, M.; Handa, S. S.; Yadav, P. P.; Mishra, P. K. Constituents of Pterocarpus marsupium: an ayurvedic crude drug. *Phytochemistry* **2004**, *65*, 915−920.

(2) Mahabusarakam, W.; Deachathai, S.; Phongpaichit, S.; Jansakul, C.; Taylor, W. C. A benzil and isoflavone derivatives from Derris scandens Benth. *Phytochemistry* **2004**, *65*, 1185−1191.

(3) Wadkins, R. M.; Hyatt, J. L.; Wei, X.; Yoon, K. J. P.; Wierdl, M.; Edwards, C. C.; Morton, C. L.; Obenauer, J. C.; Damodaran, K.; Beroza, P. J. J.; et al. Identification and characterization of novel benzil (diphenylethane-1, 2-dione) analogues as inhibitors of mammalian carboxylesterases. *J. Med. Chem.* **2005**, *48*, 2906−2915.

(4) Hyatt, J. L.; Stacy, V.; Wadkins, R. M.; Yoon, K. J. P.; Wierdl, M.; Edwards, C. C.; Zeller, M.; Hunter, A. D.; Danks, M. K.; Crundwell, G. J. J.; et al. Inhibition of carboxylesterases by benzil (diphenylethane-1, 2-dione) and heterocyclic analogues is dependent upon the aromaticity of the ring and the flexibility of the dione moiety. *J. Med. Chem.* **2005**, *48*, 5543−5550.

(5) Mousset, C.; Giraud, A.; Provot, O.; Hamze, A.; Bignon, J.; Liu, J. M.; Thoret, S.; Dubois, J.; Brion, J. D.; Alami, M. Synthesis and antitumor activity of benzils related to combretastatin A-4. *Bioorg. Med. Chem. Lett.* **2008**, *18*, 3266−3271.

(6) Ganapaty, S.; Srilakshmi, G. V.; Pannakal, S. T.; Rahman, H.; Laatsch, H.; Brun, R. Cytotoxic benzil and coumestan derivatives from Tephrosia calophylla. *Phytochemistry* **2009**, *70*, 95−99.

(7) Harada, T.; Nakagawa, Y.; Wadkins, R. M.; Potter, P. M.; Wheelock, C. E. Comparison of benzil and trifluoromethyl ketone (TFK)-mediated carboxylesterase inhibition using classical and 3D-quantitative structure-activity relationship analysis. *Bioorg. Med. Chem.* **2009**, *17*, 149−164.

(8) Young, B. M.; Hyatt, J. L.; Bouck, D. C.; Chen, T.; Hanumesh, P.; Price, J.; Boyd, V. A.; Potter, P. M.; Webb, T. R. Structure-activity relationships of substituted 1-pyridyl-2-phenyl-1,2-ethanediones: potent, selective carboxylesterase inhibitors. *J. Med. Chem.* **2010**, *53*, 8709−8715.

(9) Shen, Y.; Feng, Z. M.; Jiang, J. S.; Yang, Y. N.; Zhang, P. C. Dibenzoyl and isoflavonoid glycosides from Sophora flavescens: inhibition of the cytotoxic effect of D-galactosamine on human hepatocyte HL-7702. *J. Nat. Prod.* **2013**, *76*, 2337−2345.

(10) Wolkenberg, S. E.; Wisnoski, D. D.; Leister, W. H.; Wang, Y.; Zhao, Z.; Lindsley, C. W. Efficient synthesis of imidazoles from aldehydes and 1,2-diketones using microwave irradiation. *Org. Lett.* **2004**, *6*, 1453−1456.

(11) Deng, X.; Mani, N. S. An efficient route to 4-aryl-5-pyrimidinylimidazoles via sequential functionalization of 2, 4-dichloropyrimidine. *Org. Lett.* **2006**, *8*, 269−272.

(12) Yu, X.; Guttenberger, N.; Fuchs, E.; Peters, M.; Weber, H.; Breinbauer, R. Diversity-Oriented Synthesis of a Library of Star-Shaped 2H-Imidazolines. *ACS Comb. Sci.* **2015**, *17*, 682−690.

(13) Pradhan, K.; Tiwary, B. K.; Hossain, M.; Chakraborty, R.; Nanda, A. K. A mechanistic study of carbonyl activation under solvent-free conditions: evidence drawn from the synthesis of imidazoles. *RSC Adv.* **2016**, *6*, 10743−10749.

(14) Zhao, Z.; Wisnoski, D. D.; Wolkenberg, S. E.; Leister, W. H.; Wang, Y.; Lindsley, C. W. General microwave-assisted protocols for the expedient synthesis of quinoxalines and heterocyclic pyrazines. *Tetrahedron Lett.* **2004**, *45*, 4873−4876.

(15) Bhosale, R. S.; Sarda, S. R.; Ardhapure, S. S.; Jadhav, W. N.; Bhusare, S. R.; Pawar, R. P. An efficient protocol for the synthesis of quinoxaline derivatives at room temperature using molecular iodine as the catalyst. *Tetrahedron Lett.* **2005**, *46*, 7183−7186.

(16) Hui, X.; Desrivot, J.; Bories, C.; Loiseau, P. M.; Franck, X.; Hocquemiller, R.; Figadere, B. Synthesis and antiprotozoal activity of some new synthetic substituted quinoxalines. *Bioorg. Med. Chem. Lett.* **2006**, *16*, 815−820.

(17) Cabrera, A.; Sharma, P.; Ayala, M.; Rubio-Perez, L.; Amézquita-Valencia, M. [(*S*)-BINAP]$PdBr_2$-catalyzed direct synthesis of 2,3-disubstituted indoles via a tandem reaction between arylamines and α-diketones. *Tetrahedron Lett.* **2011**, *52*, 6758−6762.

(18) Boström, J.; Berggren, K.; Elebring, T.; Greasley, P. J.; Wilstermann, M. Scaffold hopping, synthesis and structure-activity relationships of 5,6-diaryl-pyrazine-2-amide derivatives: a novel series of CB1 receptor antagonists. *Bioorg. Med. Chem.* **2007**, *15*, 4077−4084.

(19) Zhao, Z.; Leister, W. H.; Strauss, K. A.; Wisnoski, D. D.; Lindsley, C. W. Broadening the scope of 1, 2, 4-triazine synthesis by the application of microwave technology. *Tetrahedron Lett.* **2003**, *44*, 1123−1127.

(20) Wang, G.; Wang, J.; He, D.; Li, X.; Li, J.; Peng, Z. Synthesis and biological evaluation of novel 1,2,4-triazine derivatives bearing carbazole moiety as potent α-glucosidase inhibitors. *Bioorg. Med. Chem. Lett.* **2016**, *26*, 2806−2809.

(21) Kucukkilinc, T. T.; Yanghagh, K. S.; Ayazgok, B.; Roknipour, M. A.; Moghadam, F. H.; Moradi, A.; Emami, S.; Amini, M.; Irannejad, H. Synthesis and neuroprotective activity of novel 1,2,4-triazine derivatives with ethyl acetate moiety against H_2O_2 and Aβ-induced neurotoxicity. *Med. Chem. Res.* **2017**, *26*, 3057−3071.

(22) Ren, H.; Li, J.; Zhang, T.; Wang, R.; Gao, Z.; Liu, D. Synthesis and properties of novel perylenebisimide-cored dendrimers. *Dyes Pigm.* **2011**, *91*, 298−303.

(23) Li, H.; Tam, T. L.; Lam, Y. M.; Mhaisalkar, S. G.; Grimsdale, A. C. Synthesis of low band gap [1,2,5]-thiadiazolo [3,4-g] quinoxaline and pyrazino [2,3-g] quinoxaline derivatives by selective reduction of benzo [1,2-*c*;4,5-*c*′] bis [1,2,5] thiadiazole. *Org. Lett.* **2011**, *13*, 46−49.

(24) Yamada, H.; Ohashi, C.; Aotake, T.; Katsuta, S.; Honsho, Y.; Kawano, H.; Okujima, T.; Uno, H.; Ono, N.; Seki, S.; Nakayama, K. FET performance and substitution effect on 2,6-dithienylanthracene devices prepared by photoirradiation of their diketone precursors. *Chem. Commun.* **2012**, *48*, 11136−11138.

(25) Suzuki, M.; Aotake, T.; Yamaguchi, Y.; Noguchi, N.; Nakano, H.; Nakayama, K.-i.; Yamada, H. Synthesis and photoreactivity of α-diketone-type precursors of acenes and their use in organic-device fabrication. *J. Photochem. Photobiol., C* **2014**, *18*, 50−70.

(26) Marin, L.; Kudrjasova, J.; Verstappen, P.; Penxten, H.; Robeyns, K.; Lutsen, L.; Vanderzande, D. J.; Maes, W. Quinoxaline-based cyclo(oligophenylenes). *J. Org. Chem.* **2015**, *80*, 2425−2430.

(27) Huang, S.; Gao, T.; Bi, A.; Cao, X.; Feng, B.; Liu, M.; Du, T.; Feng, X.; Zeng, W. Revealing aggregation-induced emission effect of imidazolium derivatives and application for detection of Hg^{2+}. *Dyes Pigm.* **2020**, *172*, No. 107830.

(28) Su, Y.; Zhang, L.; Jiao, N. Utilization of natural sunlight and air in the aerobic oxidation of benzyl halides. *Org. Lett.* **2011**, *13*, 2168−2171.
(29) Chen, C.-T.; Kao, J.-Q.; Salunke, S. B.; Lin, Y.-H. Enantioselective aerobic oxidation of α-hydroxy-ketones catalyzed by oxidovanadium (V) methoxides bearing chiral, *N*-salicylidene-tert-butylglycinates. *Org. Lett.* **2011**, *13*, 26−29.
(30) Muthupandi, P.; Sekar, G. Zinc-catalyzed aerobic oxidation of benzoins and its extension to enantioselective oxidation. *Tetrahedron Lett.* **2011**, *52*, 692−695.
(31) Urgoitia, G.; Martin, R. S.; Herrero, M. T.; Domínguez, E. Palladium NCN and CNC pincer complexes as exceptionally active catalysts for aerobic oxidation in sustainable media. *Green Chem.* **2011**, *13*, 2161−2166.
(32) Urgoitia, G.; Maiztegi, A.; Martin, R. S.; Herrero, M. T.; Domínguez, E. Aerobic oxidation at benzylic positions catalyzed by a simple $Pd(OAc)_2$/bis-triazole system. *RSC Adv.* **2015**, *5*, 103210−103217.
(33) Chen, S.; Liu, Z.; Shi, E.; Chen, L.; Wei, W.; Li, H.; Cheng, Y.; Wan, X. Ruthenium-catalyzed oxidation of alkenes at room temperature: a practical and concise approach to α-diketones. *Org. Lett.* **2011**, *13*, 2274−2277.
(34) Schmidt, B.; Krehl, S.; Hauke, S. Assisted tandem catalytic cross metathesis-oxidation: in one flask from styrenes to 1,2-diketones and further to quinoxalines. *J. Org. Chem.* **2013**, *78*, 5427−5435.
(35) Su, Y.; Sun, X.; Wu, G.; Jiao, N. Catalyst-controlled highly selective coupling and oxygenation of olefins: a direct approach to alcohols, ketones, and diketones. *Angew. Chem. Int. Ed.* **2013**, *52*, 9808−9812.
(36) Song, T.; Ma, Z.; Ren, P.; Yuan, Y.; Xiao, J.; Yang, Y. A Bifunctional iron nanocomposite catalyst for efficient oxidation of alkenes to ketones and 1,2-diketones. *ACS Catal.* **2020**, *10*, 4617−4629.
(37) Saberi, D.; Hashemi, H.; Niknam, K. One-pot solvent-free synthesis of diaryl 1,2-diketones by the sequential heck oxidation reaction of aryl halides with styrenes. *Asian J. Org. Chem.* **2017**, *6*, 169−173.
(38) Jung, M. E.; Deng, G. Synthesis of α-diketones from alkylaryl- and diarylalkynes using mercuric salts. *Org. Lett.* **2014**, *16*, 2142−2145.
(39) Zhu, X.; Li, P.; Shi, Q.; Wang, L. Thiyl radical catalyzed oxidation of diarylalkynes to α-diketones by molecular oxygen under visible-light irradiation. *Green Chem.* **2016**, *18*, 6373−6379.
(40) Zhou, J.; Tao, X. Z.; Dai, J. J.; Li, C. G.; Xu, J.; Xu, H. M.; Xu, H. J. Electrochemical synthesis of 1,2-diketones from alkynes under transition-metal-catalyst-free conditions. *Chem. Commun.* **2019**, *55*, 9208−9211.
(41) Charpe, V. P.; Sagadevan, A.; Hwang, K. C. Visible light-induced aerobic oxidation of diarylalkynes to α-diketones catalyzed by copper-superoxo at room temperature. *Green Chem.* **2020**, *22*, 4426−4432.
(42) Dubovtsev, A. Y.; Shcherbakov, N. V.; Dar'in, D. V.; Kukushkin, V. Y. Nature of the nucleophilic oxygenation reagent is key to acid-free gold-catalyzed conversion of terminal and internal alkynes to 1,2-dicarbonyls. *J. Org. Chem.* **2020**, *85*, 745−757.
(43) Shen, D.; Wang, H.; Zheng, Y.; Zhu, X.; Gong, P.; Wang, B.; You, J.; Zhao, Y.; Chao, M. Catalyst-free and transition-metal-free approach to 1,2-diketones via aerobic alkyne oxidation. *J. Org. Chem.* **2021**, *86*, 5354−5361.
(44) Tada, N.; Shomura, M.; Nakayama, H.; Miura, T.; Itoh, A. Direct synthesis of 1,2-diketones by catalytic aerobic oxidative decarboxylation of 1,3-diketones with iodine and base under irradiation of fluorescent light. *Synlett* **2010**, *2010*, 1979−1983.
(45) Huang, L.; Cheng, K.; Yao, B.; Xie, Y.; Zhang, Y. Iron-promoted C-C bond cleavage of 1,3-diketones: a route to 1,2-diketones under mild reaction conditions. *J. Org. Chem.* **2011**, *76*, 5732−5737.
(46) Yuan, Y.; Zhu, H. Iodine-catalyzed synthesis of 1,2-diaryldiketones by oxidative cleavage of 1,3-diaryldiketones with DMSO. *Eur. J. Org. Chem.* **2012**, *2012*, 329−333.
(47) Zhou, P. J.; Li, C. K.; Zhou, S. F.; Shoberu, A.; Zou, J. P. Copper-catalyzed TEMPO oxidative cleavage of 1,3-diketones and β-keto esters for the synthesis of 1,2-diketones and α-keto esters. *Org. Biomol. Chem.* **2017**, *15*, 2629−2637.
(48) Chen, L.-S.; Zhang, L.-B.; Tian, Y.; Li, J.-H.; Liu, Y.-Q. Copper/Iodine-cocatalyzed C-C cleavage of 1,3-dicarbonyl compounds toward 1,2-dicarbonyl compounds. *Eur. J. Org. Chem.* **2020**, *2020*, 5523−5526.
(49) Lee, J. C.; Park, H.-J.; Park, J. Y. Rapid microwave-promoted solvent-free oxidation of α-methylene ketones to α-diketones. *Tetrahedron Lett.* **2002**, *43*, 5661−5663.
(50) Ghazanfari, D.; Najafizadeh, F.; Khosravi, F. Selective oxidation of aryl ketones to α-diketones with 4-aminoperoxybenzoic acid supported on silica gel in presence of air. *Monatsh. Chem.* **2004**, *135*, 1409−1413.
(51) Park, B.-S.; Lee, H.-M.; Cho, S.-S. Facile α-ketonization of carbonyl compounds utilizing $CuBr_2$ on alumina. *Bull. Korean Chem. Soc.* **2007**, *28*, 871−872.
(52) Qi, C.; Jiang, H.; Huang, L.; Chen, Z.; Chen, H. DABCO-catalyzed oxidation of deoxybenzoins to benzils with air and one-pot synthesis of quinoxalines. *Synthesis* **2010**, *2011*, 387−396.
(53) Jayram, J.; Jeena, V. An iodine/DMSO-catalyzed sequential one-pot approach to 2,4,5-trisubstituted-1*H*-imidazoles from α-methylene ketones. *RSC Adv.* **2018**, *8*, 37557−37563.
(54) Jayram, J.; Xulu, B. A.; Jeena, V. Iodine/DMSO promoted oxidation of benzylic Csp^3−H bonds to diketones-A mechanistic investigation. *Tetrahedron* **2019**, *75*, No. 130617.
(55) Min, H.; Palani, T.; Park, K.; Hwang, J.; Lee, S. Copper-catalyzed direct synthesis of diaryl 1,2-diketones from aryl iodides and propiolic acids. *J. Org. Chem.* **2014**, *79*, 6279−6285.
(56) Lv, W.-X.; Zeng, Y.-F.; Zhang, S.-S.; Li, Q.; Wang, H. Mild $Mn(OAc)_3$-mediated aerobic oxidative decarboxylative coupling of arylboronic acids and arylpropiolic acids: direct access to diaryl 1,2-diketones. *Org. Lett.* **2015**, *17*, 2972−2975.
(57) Chand, S.; Pandey, A. K.; Singh, R.; Singh, K. N. Visible-light-induced photocatalytic oxidative decarboxylation of cinnamic acids to 1,2-diketones. *J. Org. Chem.* **2021**, *86*, 6486−6493.
(58) Bansode, A. H.; Suryavanshi, G. Iodine-mediated oxidative rearrangement of α,β-unsaturated diaryl ketones: a facile access to 1,2-diaryl diketones. *ACS Omega* **2019**, *4*, 9636−9644.
(59) Sarrafi, Y.; Tajbakhsh, M.; Hosseinzadeh, R.; Sadatshahabi, M.; Alimohammadi, K. 2,6-Dicarboxypyridinium fluorochromate−promoted oxidation of alkyl-arenes into carbonyl compounds under nonaqueous and aprotic conditions. *Synth. Commun.* **2012**, *42*, 678−685.
(60) Cacchi, S.; Fabrizi, G.; Goggiamani, A.; Iazzetti, A.; Verdiglione, R. Copper-catalyzed oxidation of deoxybenzoins to benzils under aerobic conditions. *Synthesis* **2013**, *45*, 1701−1707.
(61) Yu, J.-W.; Mao, S.; Wang, Y.-Q. Copper-catalyzed base-accelerated direct oxidation of C−H bond to synthesize benzils, isatins, and quinoxalines with molecular oxygen as terminal oxidant. *Tetrahedron Lett.* **2015**, *56*, 1575−1580.
(62) Chebolu, R.; Bahuguna, A.; Sharma, R.; Mishra, V. K.; Ravikumar, P. C. An unusual chemoselective oxidation strategy by an unprecedented exploration of an electrophilic center of DMSO: a new facet to classical DMSO oxidation. *Chem. Commun.* **2015**, *51*, 15438−15441.
(63) Guo, Y.; Meng, J.-R.; Liu, J.-Z.; Xu, T.; Zheng, Z.-Y.; Jiang, Z.-H.; Bai, L.-P. Synthesis and biological evaluation of honokiol derivatives bearing 3-((5-phenyl-1,3,4-oxadiazol-2-yl)methyl)oxazol-2(3H)-ones as potential viral entry inhibitors against SARS-CoV-2. *Pharmaceuticals* **2021**, *14*, No. 885.
(64) Wang, N.; Han, S.; Liu, R.; Meng, L.; He, H.; Zhang, Y.; Wang, C.; Lv, Y.; Wang, J.; Li, X.; Ding, Y.; Fu, J.; Hou, Y.; Lu, W.; Ma, W.; Zhan, Y.; Dai, B.; Zhang, J.; Pan, X.; Hu, S.; Gao, J.; Jia, Q.; Zhang, L.; Ge, S.; Wang, S.; Liang, P.; Hu, T.; Lu, J.; Wang, X.; Zhou, H.; Ta,

https://doi.org/10.1021/acsomega.1c06017
ACS Omega 2022, 7, 1380−1394

W.; Wang, Y.; Lu, S.; He, L. Chloroquine and hydroxychloroquine as ACE2 blockers to inhibit viropexis of 2019-nCoV Spike pseudotyped virus. *Phytomedicine* **2020**, *79*, No. 153333.
(65) Chen, R. H.; Yang, L. J.; Hamdoun, S.; Chung, S. K.; Lam, C. W.; Zhang, K. X.; Guo, X.; Xia, C.; Law, B. Y. K.; Wong, V. K. W. 1,2,3,4,6-Pentagalloyl glucose, a RBD-ACE2 binding inhibitor to prevent SARS-CoV-2 infection. *Front. Pharmacol.* **2021**, *12*, No. 634176.
(66) Zhang, G.; Pomplun, S.; Loftis, A. R.; Tan, X.; Loas, A.; Pentelute, B. L., Investigation of ACE2 N-terminal fragments binding to SARS-CoV-2 Spike RBD. *BioRxiv* **2020**.
(67) Lan, J.; Ge, J.; Yu, J.; Shan, S.; Zhou, H.; Fan, S.; Zhang, Q.; Shi, X.; Wang, Q.; Zhang, L.; Wang, X. Structure of the SARS-CoV-2 spike receptor-binding domain bound to the ACE2 receptor. *Nature* **2020**, *581*, 215−220.
(68) Ding, X.; Wu, Y.; Wang, Y.; Vilseck, J. Z.; Brooks, C. L. III, Accelerated CDOCKER with GPUs, parallel simulated annealing, and fast fourier transforms. *J. Chem. Theory Comput.* **2020**, *16*, 3910−3919.
(69) Towler, P.; Staker, B.; Prasad, S. G.; Menon, S.; Tang, J.; Parsons, T.; Ryan, D.; Fisher, M.; Williams, D.; Dales, N. A.; Patane, M. A.; Pantoliano, M. W. ACE2 X-ray structures reveal a large hinge-bending motion important for inhibitor binding and catalysis. *J. Biol. Chem.* **2004**, *279*, 17996−18007.
(70) Rao, S. N.; Reddy, N. N. K.; Samanta, S.; Adimurthy, S. I_2-Catalyzed oxidative amidation of benzylamines and benzyl cyanides under mild conditions. *J. Org. Chem.* **2017**, *82*, 13632−13642.
(71) Aruri, H.; Singh, U.; Kumar, S.; Kushwaha, M.; Gupta, A. P.; Vishwakarma, R. A.; Singh, P. P. I_2/Aqueous TBHP-catalyzed coupling of amides with methylarenes/aldehydes/alcohols: metal-free synthesis of imides. *Org. Lett.* **2016**, *18*, 3638−3641.
(72) Meesin, J.; Pohmakotr, M.; Reutrakul, V.; Soorukram, D.; Leowanawat, P.; Saithong, S.; Kuhakarn, C. TBAI/TBHP-mediated cascade cyclization toward sulfonylated indeno[1,2-*c*]quinolines. *Org. Lett.* **2017**, *19*, 6546−6549.
(73) Yan, Y.; Zhang, Y.; Zha, Z.; Wang, Z. Mild metal-free sequential dual oxidative amination of C (sp^3)-H bonds: efficient synthesis of imidazo [1,5-*a*] pyridines. *Org. Lett.* **2013**, *15*, 2274−2277.
(74) Lai, J.; Chang, L.; Yuan, G. I_2/TBHP mediated C-N and C-H bond cleavage of tertiary amines toward selective synthesis of sulfonamides and *β*-arylsulfonyl enamines: the solvent effect on reaction. *Org. Lett.* **2016**, *18*, 3194−3197.
(75) Wei, W.-T.; Zhu, W.-M.; Bao, W.-H.; Chen, W.-T.; Huang, Y.-L.; Gao, L.-H.; Xu, X.-D.; Wang, Y.-N.; Chen, G.-P. Metal-free C(sp^3)-H amination of 2-oxindoles in water: facile synthesis of 3-substituted 3-aminooxindoles. *ACS Sustainable Chem. Eng.* **2018**, *6*, 5615−5619.
(76) He, J.; Dong, J.; Su, L.; Wu, S.; Liu, L.; Yin, S. F.; Zhou, Y. Selective oxidative cleavage of 3-methylindoles with primary amines affording quinazolinones. *Org. Lett.* **2020**, *22*, 2522−2526.
(77) Luo, W.-K.; Shi, X.; Zhou, W.; Yang, L. Iodine-catalyzed oxidative functionalization of azaarenes with benzylic C(sp^3)-H bonds via *N*-alkylation/amidation cascade: two-step synthesis of isoindolo[2,1-*b*]isoquinolin-7(5H)-one. *Org. Lett.* **2016**, *18*, 2036−2039.
(78) Dhineshkumar, J.; Gadde, K.; Prabhu, K. R. Substituent-directed regioselective azidation: copper-catalyzed C-H azidation and iodine-catalyzed dearomatizative azidation of indole. *J. Org. Chem.* **2018**, *83*, 228−235.
(79) Zhang, J.; Xiao, D.; Tan, H.; Liu, W. Highly selective synthesis of 2-tert-butoxy-1-arylethanones via copper(I)-catalyzed oxidation/tert-butoxylation of aryl olefins with TBHP. *J. Org. Chem.* **2020**, *85*, 3929−3935.
(80) Montana, M.; Montero, V.; Khoumeri, O.; Vanelle, P. Quinoxaline derivatives as antiviral agents: a systematic review. *Molecules* **2020**, *25*, No. 2784.
(81) Khatoon, H.; Abdulmalek, E. Novel synthetic routes to prepare biologically active quinoxalines and their derivatives: a synthetic review for the last two decades. *Molecules* **2021**, *26*, No. 1055.
(82) Sarges, R.; Howard, H. R.; Browne, R. G.; Lebel, L. A.; Seymour, P. A.; Koe, B. K. 4-Amino[1,2,4]triazolo[4,3-*a*]quinoxalines. A novel class of potent adenosine receptor antagonists and potential rapid-onset antidepressants. *J. Med. Chem.* **1990**, *33*, 2240−2254.
(83) Hazeldine, S. T.; Polin, L.; Kushner, J.; White, K.; Bouregeois, N. M.; Crantz, B.; Palomino, E.; Corbett, T. H.; Horwitz, J. P. II. Synthesis and biological evaluation of some bioisosteres and congeners of the antitumor agent, 2-{4-[(7-chloro-2-quinoxalinyl) oxy] phenoxy} propionic acid (XK469). *J. Med. Chem.* **2002**, *45*, 3130−3137.
(84) Kim, Y. B.; Kim, Y. H.; Park, J. Y.; Kim, S. K. Synthesis and biological activity of new quinoxaline antibiotics of echinomycin analogues. *Bioorg. Med. Chem. Lett.* **2004**, *14*, 541−544.
(85) Undevia, S. D.; Innocenti, F.; Ramirez, J.; House, L.; Desai, A. A.; Skoog, L. A.; Singh, D. A.; Karrison, T.; Kindler, H. L.; Ratain, M. J. A phase I and pharmacokinetic study of the quinoxaline antitumour Agent R(+)XK469 in patients with advanced solid tumours. *Eur. J. Cancer.* **2008**, *44*, 1684−1692.
(86) Unzue, A.; Dong, J.; Lafleur, K.; Zhao, H.; Frugier, E.; Caflisch, A.; Nevado, C. Pyrrolo[3,2-*b*]quinoxaline derivatives as types $I_{1/2}$ and II Eph tyrosine kinase inhibitors: structure-based design, synthesis, and in vivo validation. *J. Med. Chem.* **2014**, *57*, 6834−6844.
(87) Smits, R. A.; Lim, H. D.; Hanzer, A.; Zuiderveld, O. P.; Guaita, E.; Adami, M.; Coruzzi, G.; Leurs, R.; de Esch, I. J. Fragment based design of new H4 receptor-ligands with anti-inflammatory properties in vivo. *J. Med. Chem.* **2008**, *51*, 2457−2467.
(88) Abu-Hashem, A. A.; Gouda, M. A.; Badria, F. A. Synthesis of some new pyrimido[2′,1′:2,3]thiazolo[4,5-*b*]quinoxaline derivatives as anti-inflammatory and analgesic agents. *Eur. J. Med. Chem.* **2010**, *45*, 1976−1981.
(89) Moreno, E.; Ancizu, S.; Pérez-Silanes, S.; Torres, E.; Aldana, I.; Monge, A. Synthesis and antimycobacterial activity of new quinoxaline-2-carboxamide 1,4-di-*N*-oxide derivatives. *Eur. J. Med. Chem.* **2010**, *45*, 4418−4426.
(90) Hu, Y.; Wang, K.; MacMillan, J. B. Hunanamycin A, an antibiotic from a marine-derived Bacillus hunanensis. *Org. Lett.* **2013**, *15*, 390−393.
(91) Guillon, J.; Mouray, E.; Moreau, S.; Mullié, C.; Forfar, I.; Desplat, V.; Belisle-Fabre, S.; Pinaud, N.; Ravanello, F.; Le-Naour, A.; Leger, J. M.; Gosmann, G.; Jarry, C.; Deleris, G.; Sonnet, P.; Grellier, P. New ferrocenic pyrrolo[1,2-*a*]quinoxaline derivatives: synthesis, and in vitro antimalarial activity-Part II. *Eur. J. Med. Chem.* **2011**, *46*, 2310−2326.
(92) Niknam, K.; Saberi, D.; Mohagheghnejad, M. Silica bonded *S*-sulfonic acid: a recyclable catalyst for the synthesis of quinoxalines at room temperature. *Molecules* **2009**, *14*, 1915−1926.
(93) Xu, T.; Zheng, Z.; Guo, Y.; Bai, L. P. Semisynthesis of novel magnolol-based Mannich base derivatives that suppress cancer cells via inducing autophagy. *Eur. J. Med. Chem.* **2020**, *205*, No. 112663.
(94) Zhou, X.; Chen, M.; Zheng, Z.; Zhu, G.-Y.; Jiang, Z.-H.; Bai, L.-P. Synthesis and evaluation of novel 12-aryl berberine analogues with hypoxia-inducible factor-1 inhibitory activity. *RSC Adv.* **2017**, *7*, 26921−26929.
(95) Dubovtsev, A. Y.; Dar'in, D. V.; Krasavin, M.; Kukushkin, V. Y. Gold-catalyzed oxidation of internal alkynes into benzils and its application for one-pot synthesis of five-, six-, and seven-membered azaheterocycles. *Eur. J. Org. Chem.* **2019**, *2019*, 1856−1864.

https://doi.org/10.1021/acsomega.1c06017
ACS Omega 2022, 7, 1380−1394